Research article Enhancing Anti-tumorigenic Efficacy of Eugenol in Human Colon Cancer Cells Using **Enzyme-Responsive Nanoparticles** Nisitha Wijewantha¹, Sanam Sane², Morgan Eikanger², Ryan M. Antony², Rashaun A Potts², Lydia Lang¹, Khosrow Rezvani^{2*}, and Grigoriy Sereda^{1*} ¹ Department of Chemistry, The University of South Dakota, 414 E Clark Street, Vermillion, South Dakota 57069, United States ² Division of Basic Biomedical Sciences, Sanford School of Medicine, The University of South Dakota, 414 E. Clark Street, Lee Medical Building, Vermillion, South Dakota 57069, United States *Corresponding author: Dr. Grigoriy Sereda, Department of Chemistry, The University of South Dakota, 414 E Clark Street, Vermillion, South Dakota 57069, United States, Phone: (605) 658-6739, FAX: (605) 677-6397 Grigoriy.sereda@usd.edu and Dr. Khosrow Rezvani, Division of Basic Biomedical Sciences, Sanford School of Medicine, The University of South Dakota, 414 E. Clark Street, Lee Medical Building, Vermillion, SD 57069, Telephone: 605-658-6383, Fax: 605-658-6383, E-mail: khosrow.rezvani@usd.edu Running title: Nanoparticles-Eugenol, an effective targeted therapy Keywords: Drug-delivery system, Nanoparticles, Eugenol, Colon cancer cells, Apoptosis

Simple Summary

37

- The migratory and invasive pathways that evolved in the early stage of colorectal cancer (CRC)
- is key to developing the metastatic cascade and drug resistance. Natural plant-based
- 40 compounds and their active secondary metabolites selectively target several oncogenic and
- 41 onco suppressive signaling pathways. The anti-cancer mechanisms medicated by plant-based
- 42 compounds allow them to circumvent the associated side effects observed with
- 43 chemotherapeutic agents. This study has developed a new potential anticancer therapeutic -
- casein-coated nanoparticles (NPs) encapsulating eugenol (EUG), a potent anti-metastatic
- 45 molecule. The active form of matrix metalloproteinases (MMPs) predominantly releases at the
- leading edges of migrating tumor cells and can locally digest the "gate-keeping" casein coat of
- 47 the EUG-carrying NPs and expose CRC cells to a high local concentration of EUG. Therefore,
- 48 the targeted delivery of EUG by a "smart" nanoparticle can significantly improve its therapeutic
- 49 index while minimizing its side effects on normal cells.

Abstract

50

- This study is focused on the selective delivery and release of the plant-based anti-cancer
- compound eugenol EUG in colorectal cancer cells (CRC). EUG is an apoptotic and anti-growth
- 54 compound in diverse malignant tumors, including CRC. However, EUG's rapid metabolization
- and excretion and its side effects on normal cells at higher dosages are major limitations of its
- therapeutic potential. To address this problem, we developed a "smart" enzyme-responsive
- 57 nanoparticle (eNPs) loaded with EUG that' exposes tumors to a high level of the drug while
- 58 keeping its concentration at the healthy cells low. We demonstrated that EUG induces apoptosis
- 59 in CRC cells irrespective of their grades in a dose- and time-dependent manner. EUG
- 60 significantly decreases cancer cell migration and invasion and the population of colon cancer
- stem cells, two key players in tumor metastasis and drug resistance. The casein-coated NPs-
- 62 EUG show a high affinity to cancer cells with rapid internalization, with no affinity toward normal
- colon epithelial cells. NPs-EUG enhanced the therapeutic efficacy of EUG measured by a cell
- viability assay and showed no toxicity effect on normal cells. The development of eNPs-EUG is
- a promising strategy for innovative anti-metastatic therapeutics.

Introduction

Natural plant extracts such as camptothecin [1] and vinblastine [2] are examples of successful anti-cancer agents entering the clinic [3]. Naturally derived anti-cancer compounds and their metabolites can target different signaling pathways and cellular mechanisms while generating fewer side effects than current genotoxic drugs such as 5-Fluorouracil (5-FU) [3, 4]. However, plant-based molecules also have adverse effects which limit their therapeutic benefits [5]. Nanotechnology has become an effective and selective local drug delivery tool for cancer treatments in the last decade [6]. The release of natural compounds from their enzymeresponsive nanoparticle carriers (eNPs) can be predictively and selectively triggered by specific enzymes expressed in tumor tissues, resulting in a safe and effective targeted delivery of anti-tumor drugs. Therefore, the eNPs can reduce systemic toxicity while enhancing the drug's therapeutic effect due to the precisely engineered concentration pattern of the drug in the body [7].

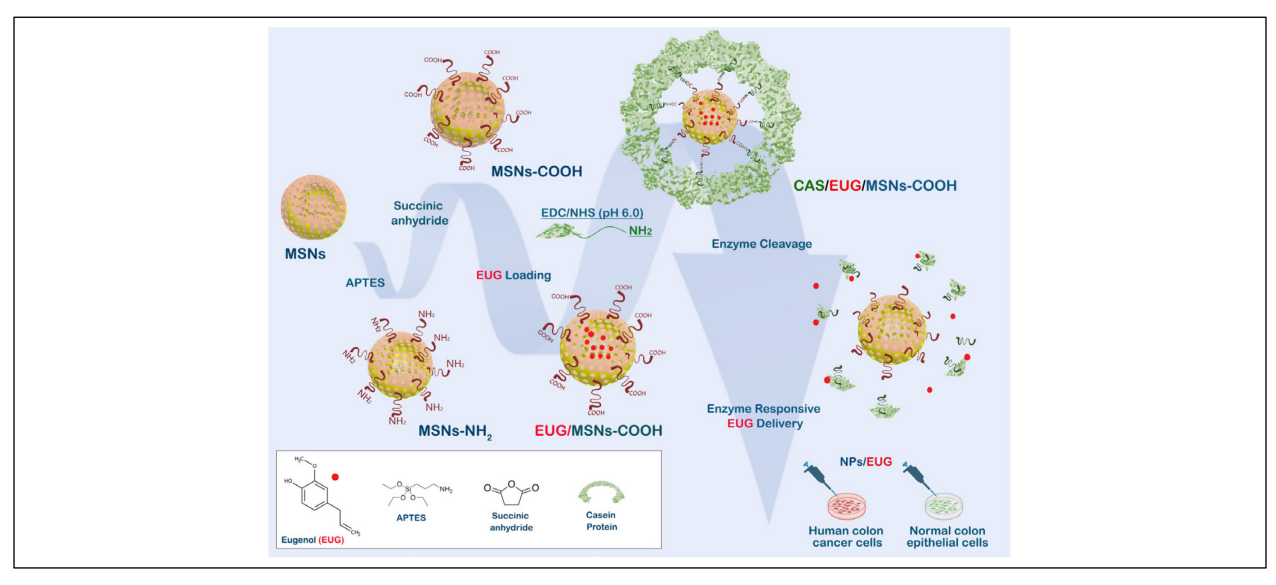
Eugenol, 2-methoxy-4-(2-propenyl)phenol, is a naturally occurring phenolic compound that is one of the main components of clove oil and honey [8]. Eugenol is traditionally used in Asian medicine due to its biological and medicinal properties, where it has been employed to treat dental and digestive disorders [9] and as an antimicrobial [10], antioxidant [11], anti-inflammatory, antiseptic, and analgesic agent [12]. The use of EUG for humans has been approved by the Food and Agriculture Organization (FAO) and World Health Organization (WHO) [13]. Furthermore, recent reports revealed that EUG had demonstrated anti-cancer activity against several cancers, including liver, colon, and breast cancers [9, 10, 12, 14], where EUG prevents cancer progression *via* modulating pathways implicated in cell growth, apoptosis, and angiogenesis [14]. However, whether EUG can suppress key elements contributing to tumor metastasis and drug resistance in CRC remained undefined.

EUG has a rapid metabolization and excretion in the urine within 24 h [15]. In normal cells, oxidative stresse and DNA damage induced by EUG, particularly at high concentrations, have been two major limiting factors for the EUG's therapeutic benefits in patients with cancer [16-18]. The short bioavailability and adverse effects have halted EUG from developing into a potent plant-based anti-cancer therapy in patients with cancers, including CRC.

We n developed a mesoporous silica nanoparticle-based system designed to deliver an anti-cancer drug molecule to target CRC cells selectively. Among many other drug-delivery nanocarriers, mesoporous silica nanoparticles (MSNs) have gained significant recognition over the last two decades [19-22] due to the MSN's well-ordered internal mesoporous structure (typically ca. 2–6 nm) with large pore volume (0.6–1 cm³/g), high surface area (700–1000 m²/g),

and tunable size (50–200 nm) [23-27]. High drug loading capacity, presence of the gate-like scaffolds, easy surface modification, shape, and robustness are ideal for using MSNs in site-specific drug delivery systems [20, 28, 29]. Moreover, zero premature release is a remarkable property of end-capped MSN drug delivery systems [30]. The controlled drug release is powered by the ability of nanoparticles to hold drug molecules inside their pores capped by covalently bound "gate keeping molecules" until the "gate keeping molecules" are detached by stimuli at the specific target site, triggering drug release [26]. Among other stimuli-responsive drug release systems, enzyme-responsive, controlled-release delivery systems show promise due to their biocompatibility and quick response to biological stimuli [31, 32]. Cancer cells including metastatic CRC tumors release a specific set of matrix metalloproteinases (MMPs) necessary for their cell invasion [33]. The active form of MMPs is predominantly released at the leading edges of migrating tumor cells [34] while it is absent in the normal tissues [35]. Digestion of the "gate keeping element" of nanoparticles by MMPs selectively released by cancer cells turns MSNs into a safe and effective drug delivery system. Finally, MSNs can increase the bioavailability of their cargo by surface modification increasing their hydrophilicity [36].

This study revealed that EUG interferes with cancer cell migration and invasion while simultaneously decreasing the population of colon cancer stem cells (CSCs). We designed a targeted and enzyme-responsive drug delivery system, "EUG/CAS-MSNs-COOH," in which MSNs were used as a vehicle to carry an anti-cancer drug (EUG) and casein was covalently attached to MSNs by the coupling of modified MSN surface's carboxy-groups with casein's amino groups (Figure 1). The EUG loading capacity of the nanoassembly was investigated *in vitro* and at the cellular level. EUG/CAS-MSNs-COOH was introduced as a promising drug delivery system for targeted primary and metastatic CRC.



- 126 Figure 1: Design and functioning of the nanoassembly for targeting colon cancer cells. MSN is modified by carboxy-
- groups, loaded with EUG, and covalently sealed by casein. Digestion of casein by MMPs released by cancer cells
- maximizes toxicity of EUG against cancer cells while protecting healthy cells.

129 Materials and Methods

- 130 Cell culture
- The colon cancer cells (HCT-116, SW480, SW620, HT29) and FHC (CRL-1831) human normal
- colon epithelial cell line were purchased from American Type Culture Collection (VA, USA) and
- grew them in the recommended medium. All examined cell lines were in passages limited to 10
- and, per the manufacturer's protocol, were routinely checked for mycoplasma contamination
- using the PCR mycoplasma detection kit (ABM).
- 136 Western Blot, immunofluorescent, and crystal violet staining method assays
- 137 Cell lysates were prepared using a digitonin lysis buffer (50 mM Tris/HCl, pH 7.5, 150 mM NaCl,
- 138 1% Digitonin (Sigma-Aldrich, St. Louis, MO) plus 1x mammalian complete protease inhibitor
- 139 (Research Products International Corp). Following homogenization (two hours of gentle rocking
- at 4°C), cell lysates were subjected to centrifugation at 13000 RPM for 10 min at 4°C, and the
- supernatant was transferred to a fresh tube in preparation for WB. Cell lysates used in WB were
- normalized for equal loading by NanoDrop using direct absorbance at 280 nm (ThermoFisher
- Scientific). The samples were loaded onto SDS-PAGE 4-20% gradient gel, and the protein
- transfer was performed using an iBlot 2 system for probing with the corresponding antibodies.
- Anti-MMP7 (Santa Cruz MMP-7 Antibody, catalog number: sc-515703, dilution 1:500) and β-
- tubulin (Proteintech, catalog number: 66240-1-lg, dilution 1:2000). Immunofluorescent assays
- were conducted as previously described [37]. The cytotoxicity test protocol using a crystal violet
- staining method has been described previously [38] using a commercial kit provided by abcam
- (Crystal violet Assay Kit or Cell viability, catalog number#ab232855).
- 150 Flow cytometry analysis
- A BD Accuri™ C6 plus cell cytometer with 488nm and 640nm excitation lasers were used for all
- 152 flow cytometry analysis according to the manufacturer's standard protocols (BD Biosciences, San
- Jose, CA). Colon cancer cell lines were analyzed by flow cytometry to determine the apoptotic
- markers (propidium iodide (PI), Annexin, and caspase 3) and the population of CD44⁺, CD133⁺,
- and Lgr5⁺ following respective antibody staining protocols provided by the manufacturers (BD
- Biosciences and Novus Biological). See the supplementary table 1 for a detailed list of fluorescent
- antibodies used in this experiment. An intracellular staining flow cytometry kit (catalog number:
- BP2-29450) and a cell surface staining flow cytometry kit (catalog number: nbp2-26247) were
- purchased from Novus Biologicals. Data were analyzed using FlowJo v10.8 (BD Biosciences).

xCELLigence real-time cell analysis

160

161

162

163

164

165

166

167168

169

170

171

172

190

191

192

xCELLigence Real-Time Cell Analyzer (RTCA) system technology measured cell migration, invasion, and adhesion assays in real-time, as previously described [39]. GraphPad Prism (version 9) was used to analyze the rate of cell proliferation (slope) during a critical time window for the HCT-116 cell line in the presence and absence of 10% FBS in McCoy's 5a Medium. Cells treated with Dimethylsulfoxide (DMSO) or EUG were immediately loaded (2X10⁴ cells) into gold microelectrode plates. E-plates were used for cell adherent assay, and CIM-plates ± Matrigel were used for migration and invasion assays, respectively. xCELLigence system measured the impedance value of each well every 15 minutes for 120 hours. The outcome of measurements is a CI (cell index) value for cell adhesion, migration, and invasion. We used plots to illustrate the CI value for overtime points. As previously described [40], the critical time point for cell adhesion, migration, and invasion was approximately between 50 hours to 70 hours after starting the experiments.

173 Reagents for nanoparticle assembly

- 174 Cetyltrimethylammonium bromide (CTAB), tetraethyl orthosilicate (TEOS, 99.98%), (3175 aminopropyl) triethoxysilane (APTES), and eugenol (4-allyl-2-methoxyphenol) were purchased
 176 from Sigma-Aldrich. Casein, trypsin solution, absolute ethanol (EtOH), succinic anhydride, 1177 ethyl-3-(3-dimethyl-aminopropyl) carbodiimide hydrochloride (EDC), N-hydroxysulfosuccinimide
 178 sodium salt (sulfo-NHS), N,N-dimethylformamide(DMF), 2-(N-morpholino)ethanesulfonic
 179 acid(MES) buffer), glacial acetic acid were purchased from ThermoFisher Scientific. Chemical
- 180 reagents were of analytical grade and were used as received.

181 Instrumentation

- Scanning electron microscope [SEM, model SIGMA FE-SEM (Zeiss)] and transmission electron
- microscope (TEM) were used to characterize the morphology and size of the prepared particles.
- 184 The powder X-ray diffractometer (XRD) (model Rigaku, ultima IV) was used to analyze the phase
- distribution and structure of the prepared powder materials. Fourier transform infrared (FT-IR)
- spectroscopy (Bruker IFS Equinox 55 Spectrometer) was carried out to probe a functionalized
- particle surface. Zeta potential values and hydrodynamic diameters of the particles were obtained
- using the Malvern Zetasizer ZS nano series. The delivered drug concentration was monitored by
- 189 UV spectrometry using a UV-500 UNICAM spectrometer.

Nanoparticle synthesis and surface modification

Mesoporous silica nanoparticles (MSNs) were synthesized and surface modified according to the procedures that we have previously reported [41]. Briefly, 2.00 g of CTAB was

stirred in nanopure water, and NaOH (7ml, 2.00 M) was added to the solution while adjusting the solution temperature to 80°C. TEOS (11.477 ml) was then added dropwise (0.5ml/min) to the surfactant solution and stirred continuously for another 2h to produce a white precipitate. The resulting nanoparticles were collected by centrifugation and washed three times by ethanol followed by three times by nanopure water before being dried at 60°C overnight in an oven to produce as-synthesized MSN particles. The oven-dried product was calcined at 550°C in a furnace in air for 2 h to obtain MSN particles (1.95 g). Carboxylation of MSNs was performed in two steps as previously described [41]. First, MSNs were aminated by the reaction with (3aminopropyl) triethoxysilane (APTES). 1.00 g of MSNs were dispersed in 30 ml of absolute ethanol, followed by addition of 1 ml of APTES and 0.6 ml of glacial acetic to the mixture. After slowly stirring the mixture for 24 h at room temperature (RT), the resulting product was separated by centrifugation, washed from absolute ethanol three times, and dried at 80°C in a vacuum oven for 24 h to obtain aminated MSNs (MSN-NH₂). In the second step, the amino groups were converted into carboxylic acid groups by treating aminated MSNs with succinic anhydride. MSN-NH₂ particles (200mg) were mixed with 25 mL of a 1 mg/mL solution of succinic anhydride in DMF. The mixture was gently stirred for 24 h at RT, the resulting product was isolated by centrifugation, washed with DMF for three times. The separated product was dried at 50° C in a vacuum oven (700 mmHg) for 24 h to obtain MSN-COOH particles (195 g).

Eugenol (EUG) loading and synthesis of EUG/MSN and EUG/MSN-COOH

193

194

195

196

197

198 199

200201

202

203

204

205206

207

208209

210

211

212213

214

215

216

217

218219

220221

222

223

Eugenol was loaded to both MSN and MSN-COOH particles. The MSN or MSN-COOH particles (5mg) were soaked in a 1.5ml eugenol solution (PBS buffer, pH 7.4) at given concentrations (and dispersed on a rotary mixer for 24h at RT. The obtained solution was centrifuged (11000 RPM, 8 min) to remove unloaded EUG. The EUG-loaded particles were washed three times with 1.5 ml PBS buffer (pH 7.4, 0.1 M) to remove the surface adsorbed EUG, resulting in the production of EUG/MSNs and EUG/MSNs-COOH from MSNs and MSNs-COOH, respectively. To determine drug encapsulation efficiency (DEE) and drug loading efficiency (DLE) of EUG for particles, all washing supernatants were collected, and the amount of free EUG was determined spectrophotometrically at λ_{max} 280nm with the aid of a calibration curve of known concentrations of EUG solutions. The DEE and DLE of eugenol for particles were calculated as follows.

DEE=
$$\frac{\text{fed drug (µg)- drug in the supernatant (µg)}}{\text{fed drug (µg)}} \times 100$$

Conjugation of casein protein to EUG/MSNs-COOH

To covalently conjugate casein with the nanoassembly, EUG/MSNs-COOH (5 mg) were dispersed in 1 mL of MES buffer (0.1 M, pH 6.0). Next, 24 µL of 250 mM EDC in nanopure water and 240 µL of 250 mM sulfo-NHS (in 0.1 M MES buffer, pH 6.0) were quickly added to the EUG/MSNs-COOH suspension. The suspension was incubated by mixing on a rotary wheel for 30 min at RT. The resulting particles were centrifuged (8000 RPM, 8 min) and gently washed with 1 mL MES buffer (pH 6.0) to remove excess EDC and sulfo-NHS. The collected particles were redispersed in 400 µL of PBS buffer (0.1 M, pH 7.4), followed by the addition of casein (1 mL of 0.1 M PBS buffer, pH 7.4) solution at given concentrations (0.1%, 0.2%, 0.3%, 0.4%, 0.5%, 0.6%, 0.7%, and 0.8%, w/v). The suspension was mixed for 5 h on a rotary mixer at RT to attach amino groups of casein to the carboxylic groups of EUG/MSNs-COOH. Finally, casein-capped drugloaded particles (EUG/CAS-MSNs- COOH) were centrifuged and rinsed with PBS buffer (pH 7.4) twice to remove the excess casein. The combined supernatants were analyzed by a BCA assay to determine the extent of conjugation with casein.

In vitro eugenol (EUG) release measurements

In vitro stimuli-responsive release of EUG from the casein-capped nanoassemblies without (control series) and in the presence of a release trigger (enzyme or(and) pH) at RT was performed by measuring the UV-vis absorption time profile at λ =280nm (λ _{max} of EUG) in the supernatant after separation of the solid nanoassemblies by centrifugation over the period of 24 h.

Control experiment series: EUG/CAS-MSNs-COOH (5mg) were dispersed separately in each of the 1.5 mL portions of 0.1 M PBS buffer adjusted to pH 7.4, 6.0, 1.5, respectively at RT. The suspension was kept homogeneous by placing it in a rotary mixer throughout the experiment. The suspension was centrifuged (8000 RPM, 8 min) to separate the nanoassemblies at the specified time points (sampling times). A 300 μ L portion of the supernatant was collected to monitor the EUG release through absorbance at λ = 280 nm. Separated nanoassemblies were resuspended, and after immediately adding 300 μ L of fresh PBS buffer to the suspension, the mixing was continued until the next sampling point.

Enzyme responsiveness: To quantify the enzyme-responsive release of EUG from EUG/CAS-MSNs-COOH, 5mg of EUG/CAS-MSNs-COOH was dispersed in 1.1 mL of 0.1 M PBS buffer solution (pH 7.4) followed by addition of 0.4 mL of trypsin solution (0.1 M PBS) of a specified

concentration at RT. The sampling of EUG concentrations was conducted as in the control experiment series. Time was set as zero when the trypsin solution was added to the suspension of casein-capped drug-loaded particles. The EUG release profile was observed over 24 h. A series of trypsin-concentrated solutions (400 μ L) in 0.1 M PBS buffer (pH 7.4) was used to determine the optimum trypsin concentration, further increasing of which does not substantially increase the EUG release.

All the EUG release studies were performed in triplicates to obtain standard deviation values for each recorded data, and the following equation determined the cumulative percentage of the released EUG:

Cumulative percentage release = $\frac{\text{EUG release at time t} + \Sigma \text{ withdrawn EUG before time t}}{\text{total EUG loaded into particles}} \times 100$

256

257

258

259260

261

262263

264

265

266

267

268269

270271

272

273274

275

276

277

278279

280281

282

283

284285

286

Results

EUG induces apoptosis in colon cancer cells

Small molecules with pro-apoptotic activities have shown strong potential value in cancer drug discovery [42], particularly natural alkaloid products [43, 44]. EUG-dependent apoptosis has been reported in various human cancer cells, including human colon cancer [45-47]. We decided first to confirm whether EUG can induce early and late apoptosis in HCT-116 cells in a time- and dose-dependent manner. The human colorectal carcinoma cell line, HCT-116, was used for apoptosis assay since this CRC cell line is a highly aggressive cell line with little or no capacity to differentiate, suggesting that HCT-116 cells are predominantly cancer stem cells (CSCs) [48]. Based on previous reports [46], HCT-116 cells were incubated with 125, 250, and 500μM EUG for 24 hours, followed by Pl/annexin-V flow cytometry analysis. Panels A-F in Figure 2 shows that EUG significantly increases the population of HCT-116 cells in early and late apoptosis. Interestingly, 125 and 250µM EUG significantly increase the population of cells in the early apoptosis (box Q3 in Figure 2B-C) and blue and green columns in Figure 2E. We saw the highest early apoptosis with 500µM EUG (purple column in Figure 2E). However, 500μM EUG significantly pushes HCT-116 cells into late apoptosis (box Q2 in Figure 2D) and the purple column in Figure 2F. We concluded that EUG induces early and late apoptosis in a dose-dependent manner (Figure 2 E and F). The mean percentages of early apoptosis are as follows: DMSO (2.75%), EUG 125μM (21.7%), EUG 250μM (31.45%), and EUG 500μM (50.40%), with a P-value of <0.05 to <0.0001 (N=4). The mean percentages of late apoptosis

are as follows: DMSO (1.75%), EUG 125μM (16.63%), EUG 250μM (34.8%), and EUG 500μM (43.82%), with a P-value of <0.01 to <0.001 (N=4). Panels A-F in Figure 2 indicate that delivery of a high dose of EUG is necessary for successful irreversible apoptosis in CRC cells. In the second set of experiments, HCT-116 cells were subjected to EUG 500μM treatment for 24, 48, and 72 hours followed by Pl/annexin-V flow cytometry analysis. Panels G-I in Figure 2 shows that EUG significantly increases the population of HCT-116 cells in the late apoptosis in a time-dependent manner. The mean percentages of early apoptosis are as follows: EUG 24 hours (51.45%), 48 hours (28.07%), and 72 hours (7.05%), with a P-value of <0.0001 (N=4). The mean percentages of late apoptosis are as follows: EUG 24 hours (42.17%), 48 hours (67.1%), and 72 hours (83.32%), with a P-value of <0.0001 (N=4). As previously reported in breast cancer [47], EUG activates apoptosis in a caspase-3-dependent manner. Panels J-M in revealed EUG 500μM significantly increases the level of caspase-3 in HCT-116 colon cancer cells. The mean percentages of caspase-3 are as follows: DMSO (30.3%) and 500μM (89.4%) with a P-value of <0.0001 (N=4). Figure 2 indicates that degradable controlled release of a high dose of EUG is necessary for successful irreversible apoptosis in CRC cells.

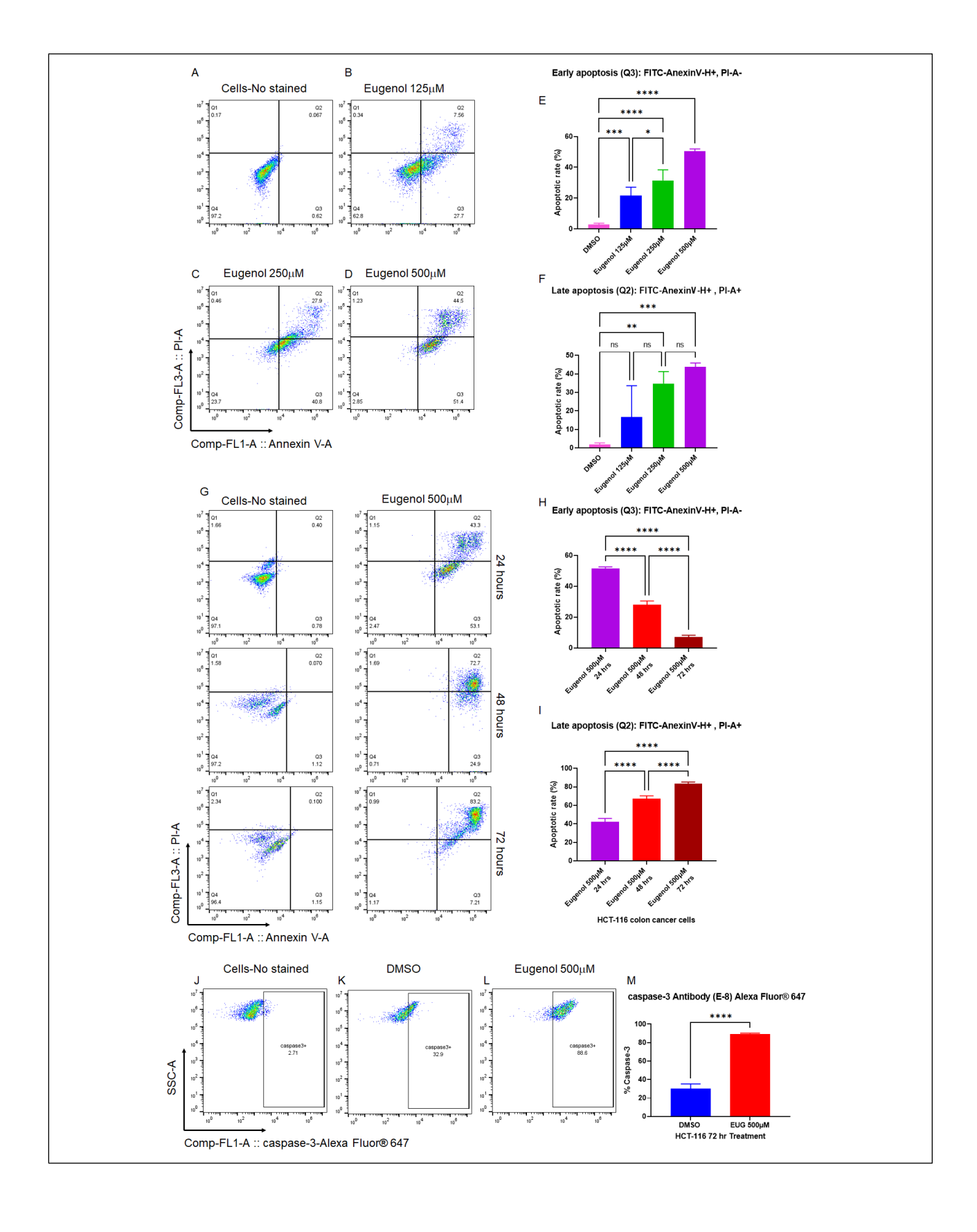


Figure 2: EUG induces apoptosis in colon cancer cells in a dose- and time-dependent manner. Panels A-F: HCT-116 colon cancer cells were incubated with DMSO or EUG (125, 250, and 500μM) for 24 hours, followed by Pl/annexin-V flow cytometry analysis. Panels G-I: HCT-116 cells were subjected to EUG 500μM treatment for 24, 48, and 72 hours followed by Pl/annexin-V flow cytometry analysis. Collected flow-cytometry results were analyzed by FlowJo software to determine the % of Annexin V-positive (early apoptosis) versus Annexin V/PI-positive cell populations in the presence and the absence of EUG. Graphical representation of FlowJo results in early and late apoptosis performed and expressed as the mean ± standard deviation. Panel J-M: Cancer cells positively stained with caspase-3 Antibody-Alexa Fluor 647 show EUG significantly increases caspase-3, a principal marker of apoptosis. Four independent experiments were done in triplicate (P-value *<0.05, **<0.01, ***<0.001, ****<0.0001).

318 319

320

321

322

323

324

325

326 327

328

329330

331

332

333

334

335

336

337

338339

307

308

309

310

311

312

313 314

315

316

317

EUG induces apoptosis in metastatic colon cancer cells:

To validate the apoptotic results achieved in Figure 2 and to determine whether EUG can induce apoptosis in metastatic colon cancer cell lines, the colon cancer cell lines SW480 derived from a primary tumor and SW620 from a metastatic site in the same patient [49] were treated with 125, 250, and $500\mu M$ EUG. After 24 hours, cells were subjected to Pl/annexin-V flow cytometry analysis. Measured early and late apoptosis in Figure 3 show 500μM EUG significantly induces late apoptosis in both SW480 and SW620 (purple columns in Figure 3E and F). Interestingly, early apoptosis measured in SW480 cells was not sensitive to EUG in a dose-dependent manner (Figure 3C). Early apoptosis in SW620 cells revealed a significant response to EUG 125μM and 250μM (Figure 3D). However, EUG 500μM shifted cells from early to late apoptosis in SW620 cells (purple columns in Figure 3D and F). The mean percentages of early apoptosis in SW480 are as follows: DMSO (5.95%), EUG 125μM (24.07%), EUG 250μM (24.57%), and EUG 500μM (24.5%), with a P-value of <0.0001 (N=4). The mean percentages of late apoptosis in SW480 are as follows: DMSO (2.6%), EUG 125μM (9.02%), EUG 250μM (6.65%), and EUG 500μM (57.55%), with a P-value of <0.05 to <0.0001 (N=4). The mean percentages of early apoptosis in SW620 are as follows: DMSO (3.18%), EUG 125μM (59.07%), EUG 250μM (48.12%), and EUG 500μM (29.67%), with a P-value of <0.0001 (N=4). The mean percentages of late apoptosis in SW620 are as follows: DMSO (1.18%), EUG 125μΜ (25.7%), EUG 250μM (23.27%), and EUG 500μM (62.5%), with a P-value of <0.0001 (N=4). The results in Figure 3 provide further evidence of the effective apoptotic function of EUG in CRC cells in different cancer stages suggesting a comprehensive rationale for the selective targeting of metastatic CRC tumors with a high dose of EUG.

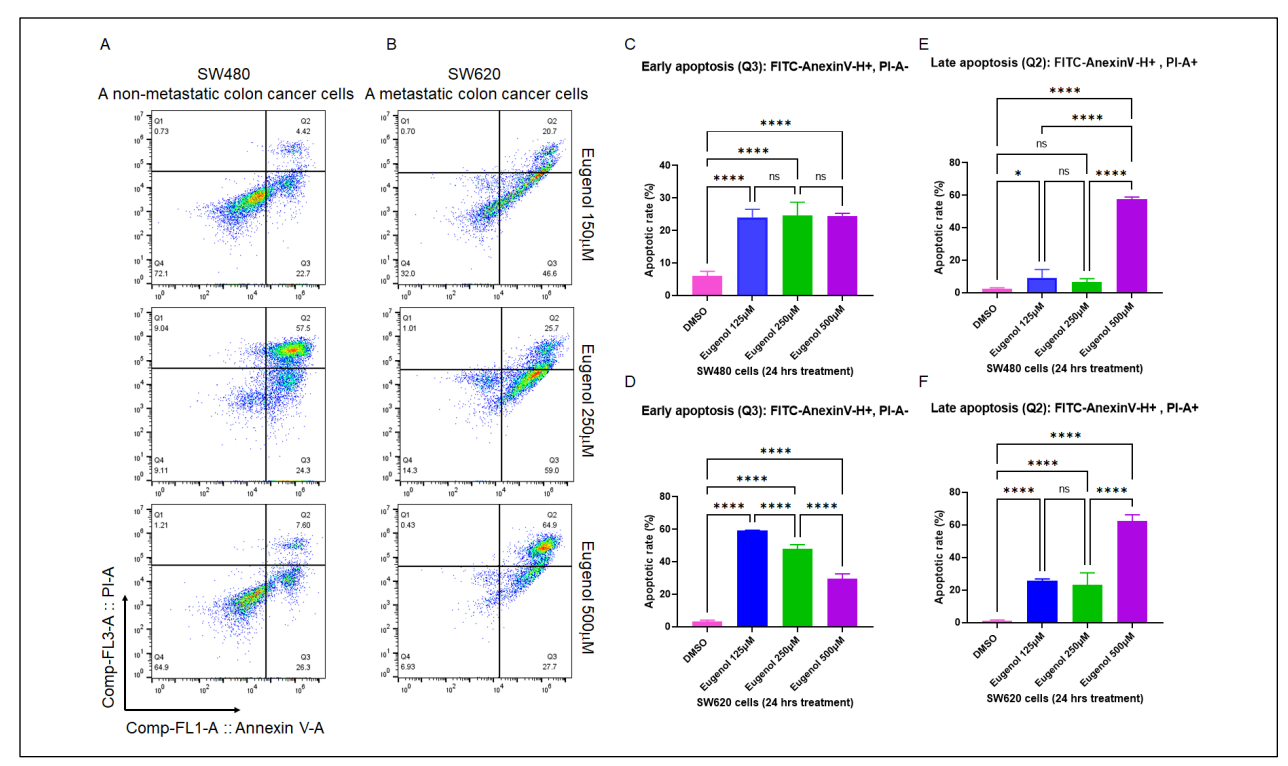


Figure 3: EUG induces apoptosis in the metastatic colon cancer cells. Panels A-F: SW480 (Primary CRC) cells and SW620 (metastatic CRC) cells were incubated with DMSO or EUG (125, 250, and 500μM) for 24 hours, followed by Pl/annexin-V flow cytometry analysis. Collected flow-cytometry results were analyzed by FlowJo software to determine the % of Annexin V-positive (early apoptosis) versus Annexin V/PI-positive cell populations in the presence and the absence of EUG. Panels A, C, and E show significant induction of late apoptosis in SW480 by 500μ M EUG. Similar significant late apoptosis signals were measured in metastatic SW620 cells in the presence of 500μ M EUG (Panel F). Meanwhile, measurement of early apoptosis (Annexin positive, PI negative) showed a sensitivity of both cell lines to EUG. (Panels C and D). Four independent experiments done in triplicate (P-value *<0.05, **<0.01, ***<0.001, ****<0.0001, mean ± standard deviation).

EUG suppresses migration and invasion in the HCT-116 colon cancer cell line

Migration and invasion are critical steps in cancer metastasis [50]. To investigate whether EUG could suppress the migration and invasion abilities of CRC cells, we used the xCELLigence Real-Time Cell Analysis detection platform to determine the rate of cell adhesion as previously described [51] (Figure 4A). HCT-116 cells received 125, 250, or 500μM EUG was immediately seeded on E-plates (cell adhesion assay) or CIM plates without Matrigel (migration assay) or with Matrigel (invasion assay) as previously described [39, 52]. Figure 4B-C shows that EUG significantly reduces the cell adhesion capacity of HCT-116 cells monitored by E-Plates (N=4, p<0.0001) in a dose-dependent manner. The recorded migration of HCT-116 cells (Figure 4D-E) and analyzed cell index (Figure 4F) show that the 500μM EUG can significantly decrease cell

365366

367

368

369

Figure 4: EUG significantly reduces cell adhesion, cell migration, and invasion in human colon cancer cells. Panel A: The xCELLigence RTCA technology is an accurate platform for non-invasive measurement of cell adhesion/viability and migration/invasion in live cells. HCT-116 cells were monitored in real-time for cell adhesion as well as cell migration and invasion for 120hr in the presence of EUG. Graphs (panels B, D-E, and G-H) and statistical analysis of calculated slopes (panels C, F, and I) using critical time points between 50hr to 70hr post-treatment (Blue and red lines in panel B) showed that EUG significantly suppressed cancer cell adhesion, migration, and invasion. Experiments done in the absence and the presence of serum starvation (Panels F and I) had no effect on EUG's suppressive effects, indicating that EUG targets key signaling pathways involved in migration and invasion. The blue (the 50 hours timeline) and red (70 hours timeline) in panel B show critical time point used for analyzing the cell indexes recorded in adhesion, migration, and invasion assays in live cells. Experiments were repeated two times with N of 4 per cell line per experiment (*****P<0.0001, mean ± SD).

EUG decreases population of LGR5+, CD44+, and CD133+ colon cancer stem cells

It is well-accepted that colon cancer stem cells (CSCs) are the drivers of tumor progression and drug resistance [53]. It has been shown that therapeutic doses of EUG target CSCs in breast cancer by significant downregulation of β-catenin [54, 55]. We used flow cytometry to determine whether the EUG can decrease colon CSC populations. We used LGR5, CD44, and CD133 to examine the effect of EUG on CSCs (HCT-116 cells). HCT-116 cells received 125 or 500μM EUG for 24 h. Panels 5A-E (CD44⁺), G-K (Lgr5⁺), and M-Q (CD133⁺) represent population of positive cells. Statistical analysis of recorded positive cells (panels F, L, and R in Figure 5) revealed EUG 500μM significantly decreases the level of receptor-positive CSCs among HCT-116 cells. The mean percentages of remaining positive CSCs pool in HCT-116 cells treated with 500μM are as follows: CD44⁺ (18.175%), Lgr5⁺ (1.33%), CD133⁺ (16.125%), with a P-value of <0.0001 (N=4). Both CD44 and LGR5 are involved in local and liver metastasis in colorectal cancer [56]. On the other hand, CD133 CSCs are accepted as a reliable prognostic marker in patients and as a potential target for CRC treatment [57]. In general, colon CSCs are highly tumorigenic, aggressive, and chemo resistant, and they are a critical factor in the metastasis and recurrence of CRC [58]. These data suggest that EUG can potentially suppress the CSCs at higher doses delivered by NPs, increasing the druggability of NP-EUG as an effective anti-metastatic targeted therapy.

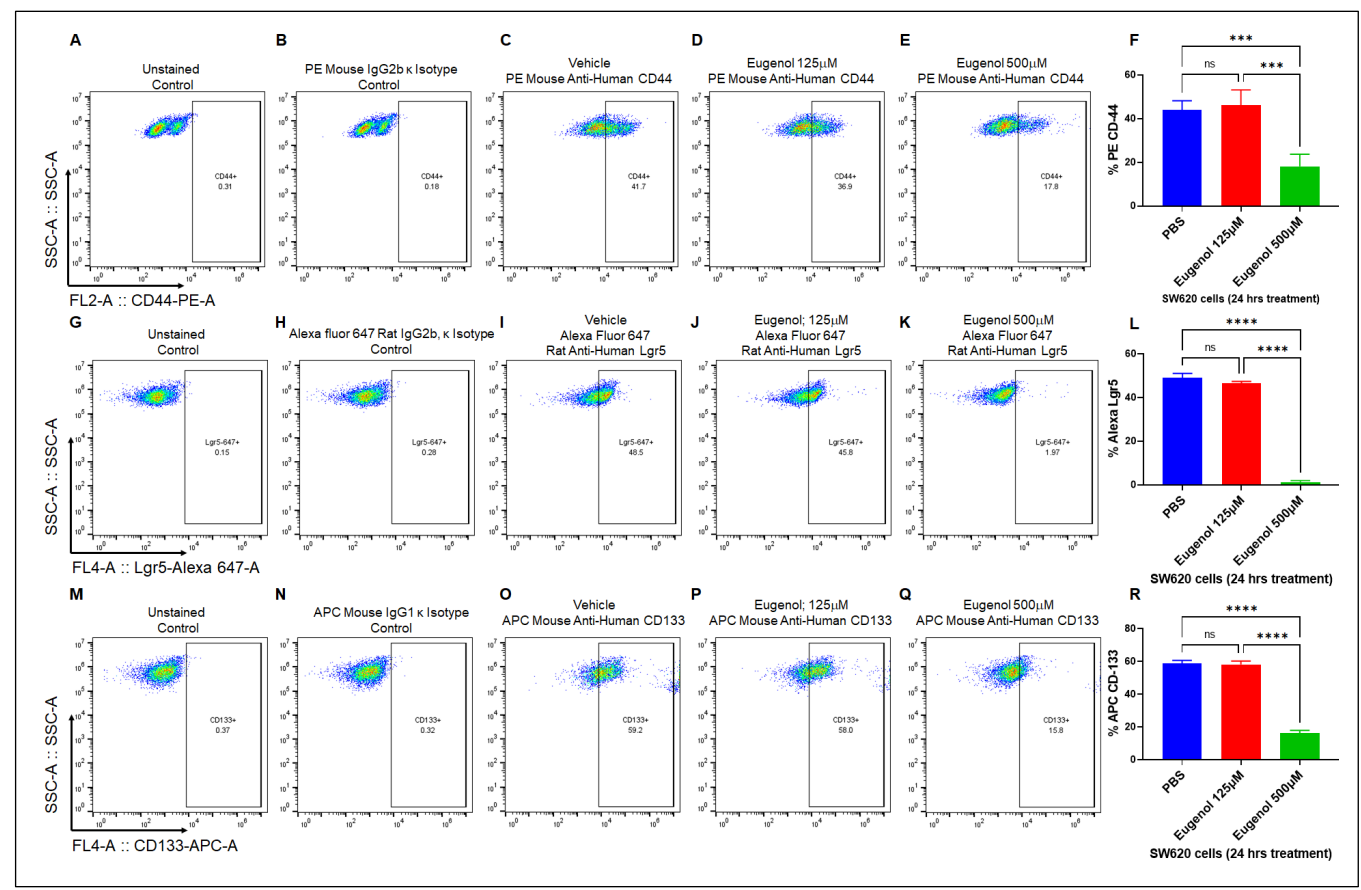


Figure 5. EUG decreases cancer stem cell populations in human colon cancer cells. CSCs positive for Lgr5, CD44, and CD133 cell populations are associated with poor prognosis and drug resistance in CRC tumors. HCT-116 colon cancer cells were treated with DMSO or EUG (125 and $500\mu M$). After 24 hours, cells were subjected to flow cytometry analysis using three CSC markers (CD44, Lgr5, and CD133). Cells treated with $500\mu M$ EUG showed a significant reduction of CD44 (A-F), LGR5 (G-L), and CD133 (M-R) (N=4, ***<0.001 **** p< 0.0001, mean +/- SD). Unstained cells and Mouse IgG2b or IgG1 Isotype controls (panels B, H and N) were used to confirm the accuracy of measurements with used antibodies.

Synthesis and characterization of casein-capped controlled eugenol delivery system

As illustrated in figure 1, MSNs-based nanoassemblies end-capped with casein were successfully fabricated and tested as a controlled eugenol delivery system. The sol-gel reaction method was used to synthesize the base material MSNs. MSNs-NH₂ were fabricated by grafting APTES on the surface of MSNs. Subsequently, MSNs-COOH were prepared by introducing succinic anhydride by acyl nucleophilic substitution, as we reported previously [41]. To covalently couple the casein to the MSNs-COOH, EDC and sulfo-NHS was added to the MSNs-COOH suspension. Then, casein was added to the suspension, and the mixture was stirred for 5h to couple the amine group of casein to the carboxyl group of nanoassemblies. The synthesized nanoassemblies were characterized by transmission electron microscopy (TEM), scanning electron microscopy (SEM), powder X-ray diffraction spectra (PXRD), Fourier transform infrared spectroscopy (FT-IR), and dynamic light scattering (DLS).

The morphology and size of the nanoassemblies were evaluated by SEM and TEM imaging (Figure. 6A). The synthesized MSN particles had a uniformly spherical shape with an average diameter of 95 nm. After covalently coupling with casein, the average diameter of nanoassemblies (EUG/CAS-MSN-COOH) increased to about 115 nm while exhibiting almost unchanged morphology (Figure 6A-subpanels a and b). The well-orderly arranged hexagonal mesopore structures are revealed on the TEM images for nanoassemblies (Figure 6A- subpanel c). The small-angle powder X-ray diffraction patterns (PXRD) for nanoassemblies further illustrated the formation of well-orderly arranged hexagonal structure from the diffraction peaks within the ranges of 2.3° to 2.35°, and 4.0° to 5.0° (20), which can be assigned to the (100), (110), and (200) diffraction planes of the unit cell. There was a decrease in peak intensity for EUG/MSNs-COOH, showing a little distortion of the ordered mesopore structure (Figure 6B). After coupling with casein, the XRD spectrum peaks for EUG/CAS-MSNs-COOH were much weaker, indicating the pores of nanoassemblies were capped by casein, which is further confirmed by the blurred pore structure from TEM images of EUG/CAS-MSNs-COOH (Figure 6A-subpanel d).

The hydrodynamic diameter, size distribution (PDI), and surface charge for nanoassemblies were evaluated by DLS analysis and zeta potential measurements. As presented in Figure 6C, the hydrodynamic diameter of MSNs, EUG/MSNs-COOH, and EUG/CAS-MSNs-COOH was approximately 191 nm (PDI-0.287), 210 nm (PDI-0.379), and 245 nm (PDI-0.313), respectively. Hydrodynamic diameter values were larger than the particle diameter exhibited on the TEM images, due to the solvation layer at the particle surface in the solution subjected to the DLS analysis. An increase of around 35 nm in average diameter for casein-capped particles after

casein conjugation confirms successful casein coupling to the particle surface. The zeta potential measurements for prepared nanoassemblies were shown in Figure 6D the zeta potential of MSNs, EUG/MSNs-COOH, and EUG/CAS/MSNs-COOH were -26.33 mV, -48.65 mV, and -58.54 mV, respectively. The silanol groups on the MSNs surface account the negative charge of the surface. The nanoassemblies gained more negatively charged groups after introduction of carboxy-groups and coupling with casein, which was reflected in their zeta-potentials.

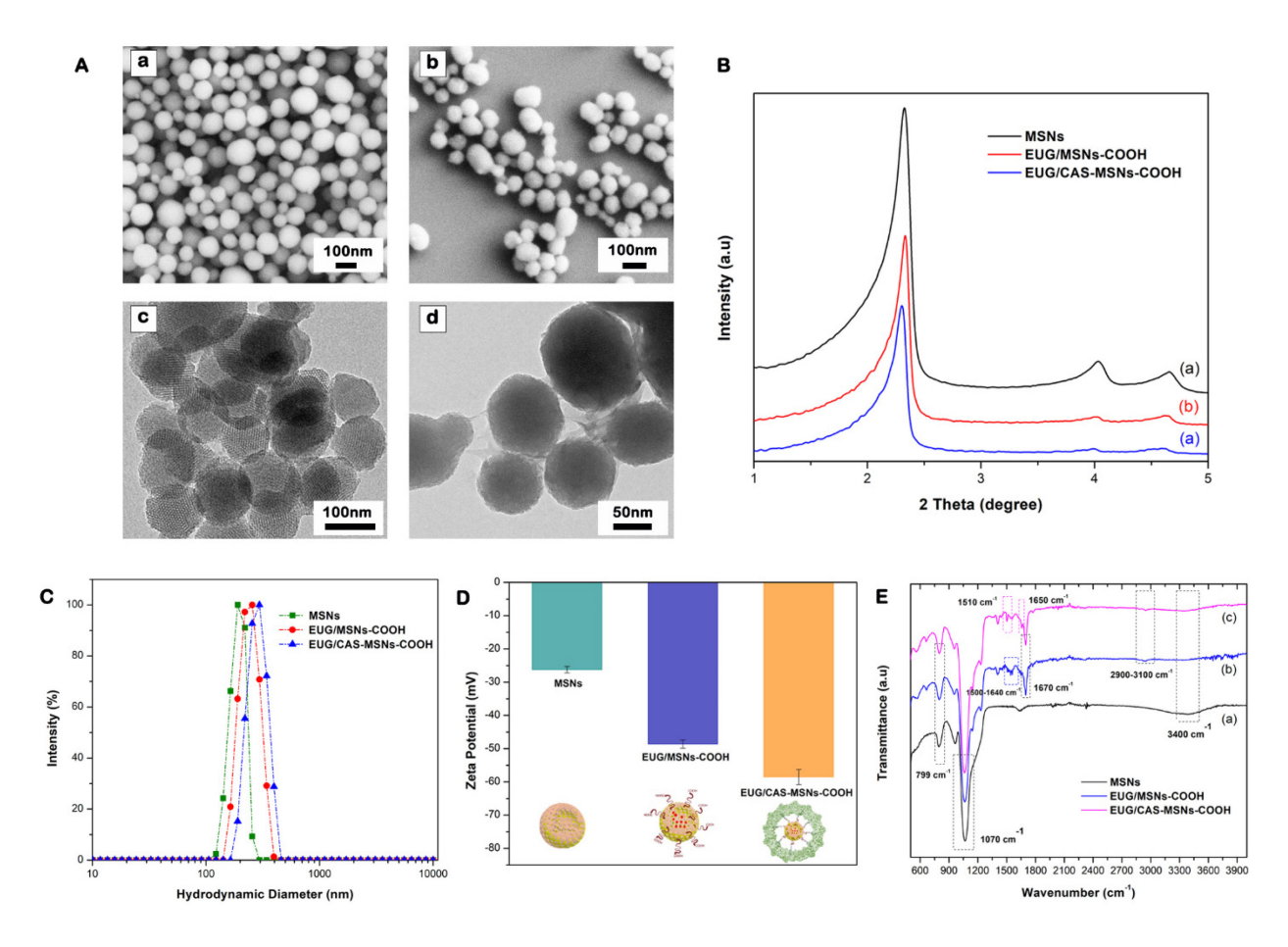


Figure 6. Synthesis and characterization of casein-capped controlled eugenol delivery system (A) SEM and TEM images, subpanels a and b illustrate SEM images of MSNs and EUG/CAS-MSNs-COOH, respectively. Subpanels c and d illustrate TEM images of MSNs and EUG/CAS-MSNs-COOH, respectively. (B) XRD patterns, (C) zeta size distribution, (D) zeta potential at pH 7.4, (E) FTIR spectra of for MSNs, EUG/MSNs-COOH, and EUG/CAS-MSNs-COOH.

Surface-incorporated layers and the presence of eugenol in MSN particles were confirmed by the FTIR spectra for MSNs, EUG/MSNs-COOH, and EUG/CAS-MSNs-COOH (Figure 6E). All FTIR spectra showed similar characteristics bands of mesoporous silica at 1070 cm⁻¹ (asymmetric Si-O-Si stretching), at 799 cm⁻¹ (symmetric Si-O stretching), 3400 cm⁻¹ (OH), and 965 cm⁻¹ (Si-OH stretching) [59, 60]. After grafting of COOH-groups to MSNs, one of the new bands appeared

at 1670 cm⁻¹ belonging to the C=O vibration of the COOH group, which confirmed the successful grafting (Figure 6E-subpanels b and c). Characteristics bands of eugenol located at (2990, 2930) cm⁻¹ (CH stretching), 1635, 1590, and 1510 cm⁻¹ (C=C aromatic ring) [61, 62]. After eugenol encapsulation, both EUG/MSNs-COOH and EUG/CAS/MSNs-COOH nanoassemblies spectra showed new characteristic peaks of eugenol, which confirmed that the eugenol was successfully encapsulated into the MSNs (Figure 6E-subpanels b, c). The intensity of the C-H stretching band between 2900 and 3100 cm⁻¹ was increased considerably for EUG-loaded particles, confirming successful eugenol encapsulation into the MSNs [61]. The presence of casein in the casein-capped MSNs surface also was confirmed by FTIR spectroscopy (Fig. 6E-subpanle c). The presence of new peaks between 1650 cm⁻¹ and 1500 cm⁻¹ for EUG/CAS-MSNs-COOH, which can be attributed to the characteristic of amide I and amide II, are present in the FTIR spectra of the synthesized casein-capped MSNs [63].

Eugenol (EUG) loading, casein coupling, and enzyme responsive *in vitro* release of eugenol

A schematic diagram of EUG loading into nanocarriers is shown in Figure 7A. In order to find out the optimal eugenol amount that can be loaded into the nanoassemblies with high drug loading amount and efficiency, a series of different eugenol (EUG) amounts containing 150, 75, 37.5, 30, 15, and 7.5 μ g was loaded into 5 mg of nanoassemblies. The calculated drug loading efficiency (DLE) and encapsulation efficiency (DEE) are presented in Figure 7B. The DLE was proportionate to the EUG concentration, while the DEE decreased with the increased EUG concentration. The optimal EUG concentration was found to be 25 μ g/ml, where DEE was high (77.2%), and DLE was 0.579%.

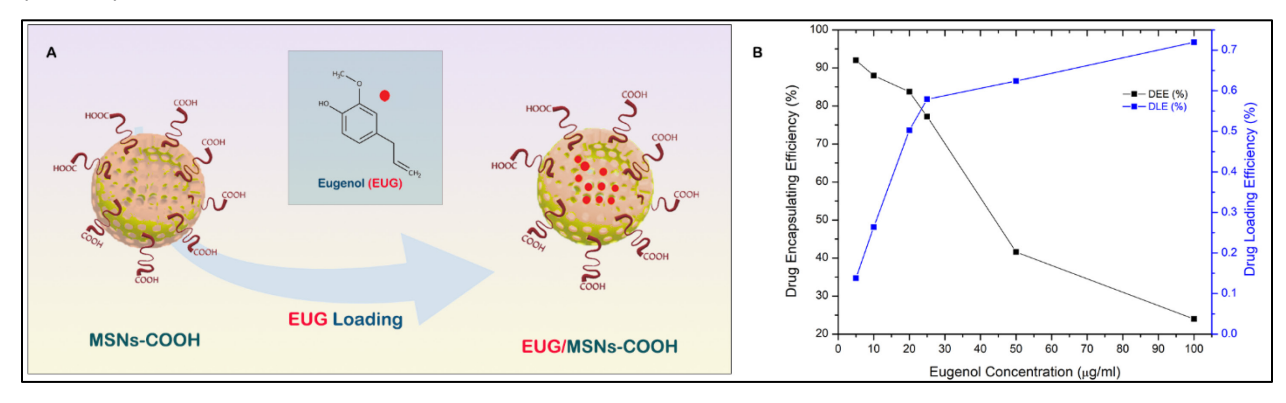


Figure 7. (A) Eugenol EUG loading into the MSN pore channels, (B) Effect of EUG concentration on drug loading efficiency (DLE) and drug encapsulation efficiency (DEE) of MSN nanoassemblies, $25 \mu g/ml$ EUG concentration was identified as the optimum concentration that was efficiently loaded to the MSN pre channels.

After obtaining the optimal EUG amount contained in the MSN nanoassemblies, we determined the optimum amount of casein required to achieve maximum EUG encapsulation inside the MSN nanoassemblies. As shown in Figure 8A, casein at given concentrations (0.1%,0.2%, 0.3%, 0.4%, 0.5%, 0.6%, 0.7%, and 0.8%, w/v) was covalently conjugated to the MSN nanoassemblies, followed by the drug-releasing experiments to determine the optimal amount of casein that can hold the maximum amount of loaded EUG inside the MSN channels for 24h. As depicted in Figure. 8B, there was no significant EUG encapsulation for 24h in the control experiment (0% casein w/v), indicating that without the pore-blocking agent of casein, eugenol was immediately released from the open pore channels of MSN nanoassemblies without a substantial retention. As the amount of the attached casein increased, there was a gradual improvement in the EUG encapsulation efficiency until casein w/v% reached 0.6% w/v. As shown in Figure 8C, 73.8% of loaded EUG was held for 24 h inside the MSN nanoassemblies after capping the pore channels with 0.6 w/v% casein. Further increase of the amount of conjugated casein resulted in only marginal increase of the EUG encapsulation efficiency, suggesting that 0.6% casein w/v was the optimal value that efficiently holds EUG for 24 h inside the MSN nanoassemblies. These observations defined our selection of using 0.6% w/v casein for synthesizing EUG/CAS-MSNs-COOH nanoassemblies for all EUG release experiments. The amount of casein conjugated to MSN nanoassemblies was determined by the Bicinchoninic acid (BCA) protein assay. In this assay, after casein conjugation, the remaining free casein in the MSN nanoassemblies dispersion was separated by centrifugation and analyzed by the BCA assay. According to the BCA assay, covalent conjugation of casein at its optimal concentration to the MSN nanoassemblies exhibited the coupling efficiency of 28.9%.

497

498

499

500

501

502

503

504 505

506

507

508

509 510

511

512513

514

515

516

517

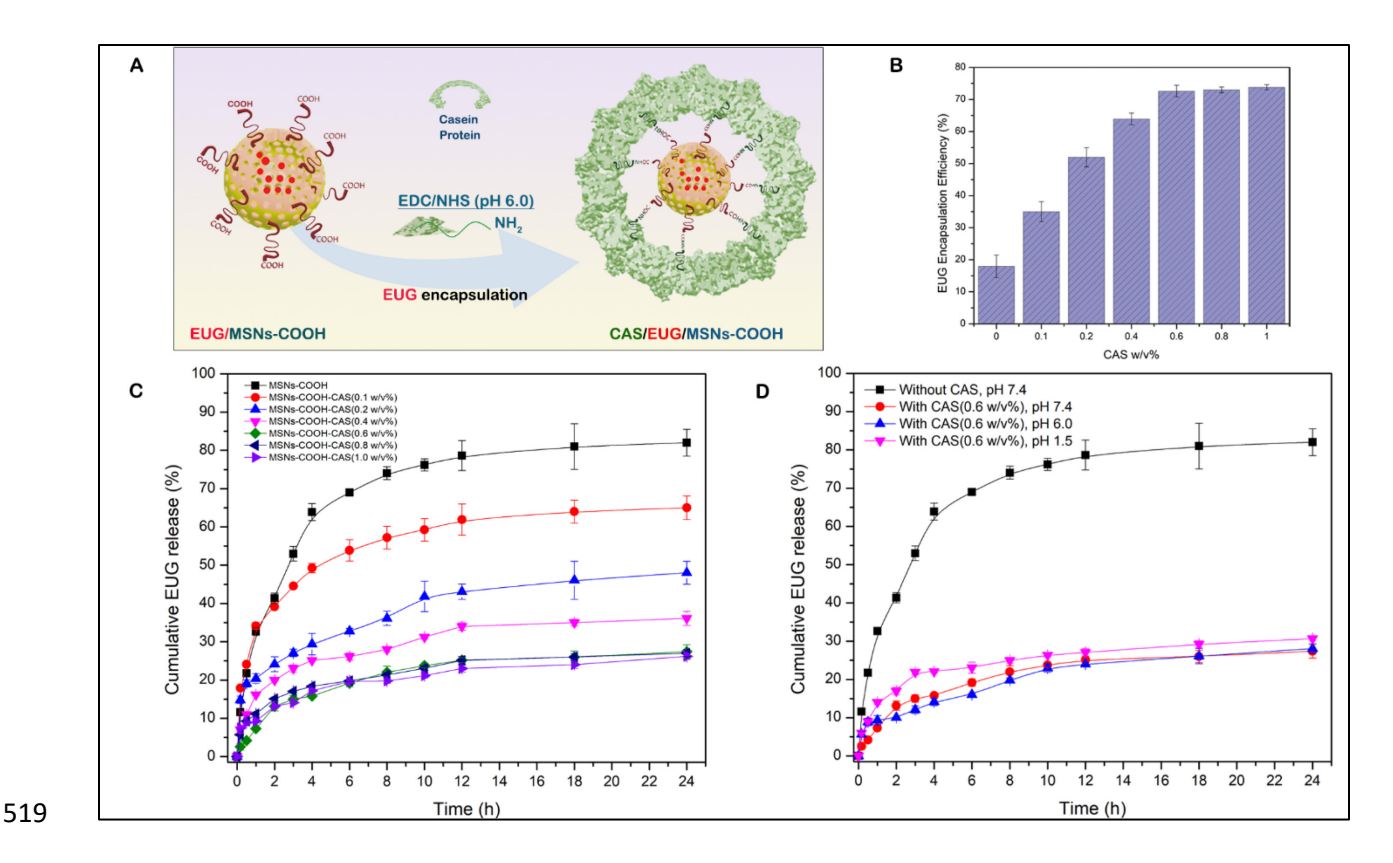


Figure 8. (A) Conjugation of casein to the carboxy-functionalized MSN particles after NHS/EDC activation, (B) The encapsulation efficiency of eugenol (EUG) for 24h along with varying w/v% of casein as a capping layer for EUG-loaded MSN nanoassemblies, (C) Cumulative release (%) profiles of EUG from EUG/CAS-MSNs-COOH at different w/v% of casein at pH 7.4, RT to obtain the effect of casein capping layer for EUG release over 24h. The black curve represents EUG release profiles without any casein conjugation to the EUG/MSNs-COOH. (D) Cumulative release (%) profiles of EUG from EUG/CAS-MSNs-COOH (0.6 w/v% casein) at different pH conditions, pH 7.4 (Red curve), pH 6.0 (Blue curve), pH 1.5 (Pink curve). The black curve represents EUG release profiles without any casein conjugation to the EUG/MSNs-COOH at pH 7.4, RT. Each data point represents the mean of the experiments performed in triplicate, along with their corresponding standard deviation.

After identifying the optimum casein w/v% for the substantial retention of EUG inside the MSN nanoassemblies, we performed drug release experiments at different pH values and demonstrated that the EUG/CAS-MSNs-COOH is able to hold the drug inside the MSNs channels at the wide pH-range (1.5 – 7.4) for 24 h in PBS. Three different pH conditions were selected to simulate the conditions of the intestine (pH 7.4) [64], colon (pH 6.0) [65], and stomach (pH 1.5) [66], and EUG release by EUG/CAS-MSNs-COOH were carried out in the absence of any enzymes at RT (Figure 8D). Therefore, casein maintains the pores sealed over the pH range of 1.5-7.4 in the absence of any enzyme.

The enzyme-responsive drug release experiments with EUG/CAS-MSNs-COOH as shown in Figure 9A. Trypsin solutions (0.4 mL) at 0%, 0.01%, 0.05%, 0.1%, 0.2%, and 0.25%

w/v% concentrations were added separately to each of the 1.1 ml portions of the PBS buffer (pH 7.4, RT), containing 5 mg of EUG/CAS-MSNs-COOH (0.6 w/v% casein) to determine the optimum concentration of trypsin that triggers significant EUG release from EUG/CAS-MSNs-COOH (Figure 9B). The time zero was set when the enzyme was added to the suspensions of the nanoassembly, and the release of EUG was monitored for 24h (Figure 9C). In the control experiment (without trypsin), only ~25% of EUG leaked over 24h from the nanoassembly. In the presence of trypsin, the cumulative release of EUG for 24 h at pH 7.4 was about 49%, 65%, 71%, 80%, and 79%, at 0.01%, 0.05%, 0.1%, 0.2%, and 0.25% w/v% trypsin concentrations respectively (Figure 9B). The time release profiles demonstrate that trypsin triggered release of EUG in the concentration-dependent manner until its concentration of 0.2 w/v%. Further increase of the trypsin con centration did not result in more efficient release of EUG from the pore channels (Figure 9B). Therefore, 0.2 w/v% is the optimum trypsin concentration that triggers ~80% release of EUG for 24h from the EUG/CAS-MSNs-COOH at pH 7.4, RT (Figure 9D).

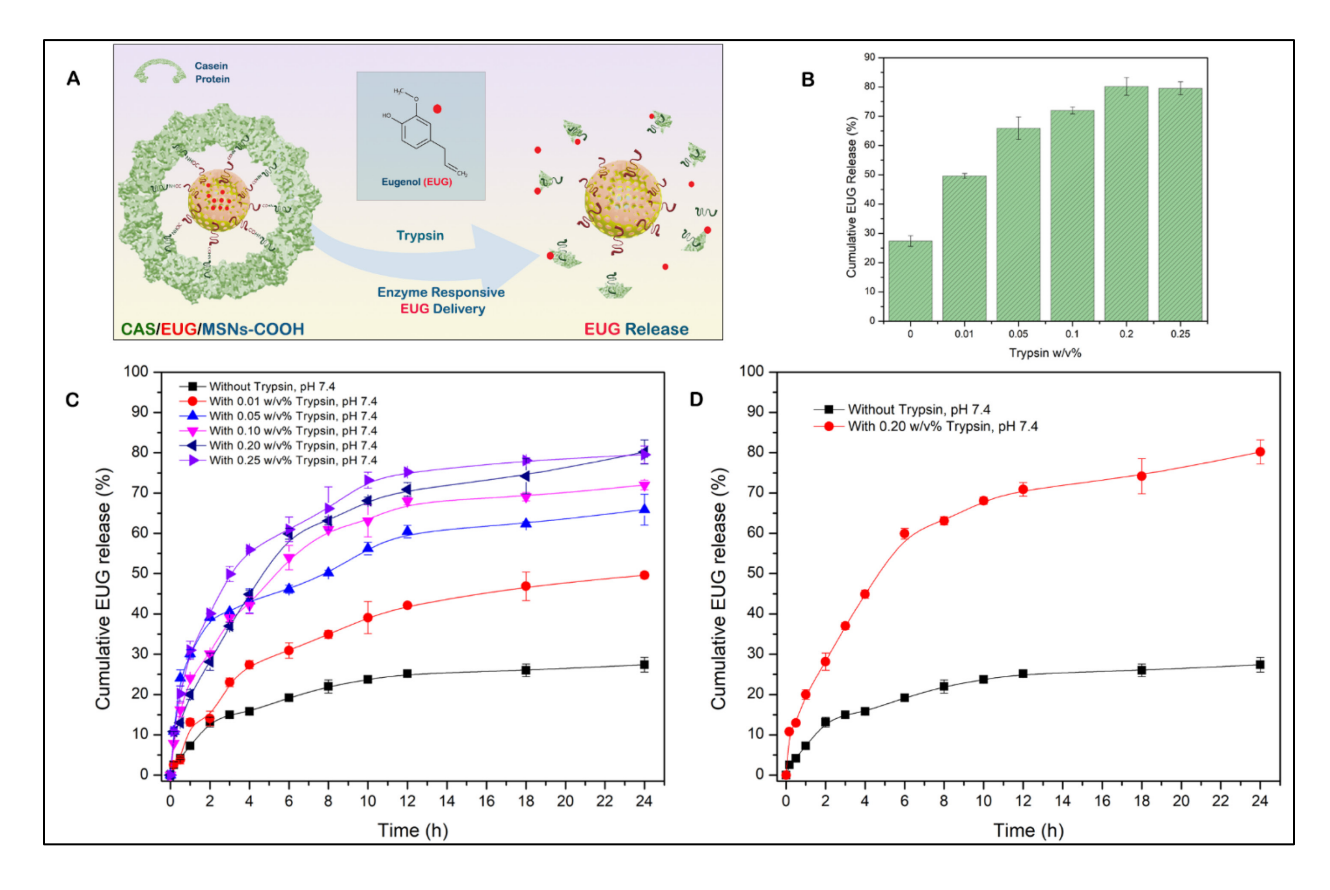


Figure 9. (A) Release of an anti-cancer drug, EUG, which is triggered by trypsin that cleaves a gatekeeping component (casein) of the EUG/CAS-MSNs-COOH, (B)The cumulative release of EUG for 24h at pH 7.4, RT at different w/v% of trypsin from the MSN-COOH pore channels, (C) Cumulative release (%) profiles of EUG from EUG/CAS-MSNs-COOH with and without trypsin at different w/v% (pH 7.4, RT) for 24h. The black curve represents EUG release

profiles from the EUG/MSNs-COOH in the absence of trypsin at pH 7.4, RT, (D) Cumulative release (%) profiles of EUG from EUG/CAS-MSNs-COOH in the presence of the 0.20 w/v% trypsin mixture (optimized concentration) (red curve) and the absence of any enzymes from casein-capped MSNs-COOH (black curve) at pH 7.4, RT. Each data point represents the mean of the experiments performed in triplicate and their corresponding standard deviation.

564565566

567

560

561 562

563

Casein-coated NPs-EUG decrease cell viability in cancer cells while normal colon epithelial cells remain intact.

The active form of matrix metalloproteinases (MMPs) is predominantly released at the leading 568 edges of migrating tumor cells [34], and they play an important role in the development and 569 progression of CRC [67, 68]. Several MMPs, including MMP-7, are overexpressed in human 570 CRC [69]. MMP-7 is substantially expressed by CRC [35, 70], and its concentration increases in 571 a stage-dependent manner in CRC [71]. In fact, MMP-7 has an approximately 6-fold greater 572 573 expression in tumor masses versus normal cells [72]. Therefore, MMP-7 can potentially be 574 utilized for the site-specific release of anti-metastatic drugs against human CRC primary and 575 metastatic tumors. Based on the current reports, we conducted a set of western blots (WBs) to 576 confirm that only colon cancer cells contain a large pool of MMP-7 (Figure 10A). HCT-116, HT-577 29 (a human-derived colorectal adenocarcinoma), FHC (a normal colon epithelial cell), and HEK 293 cell line (widely known as the Human Embryonic Kidney 293 cells) were subjected to WBs 578 579 using an anti-MMP-7 antibody. WB results revealed that HCT-116 and HT-29 contain an 580 enriched pool of MMP-7 in the cytoplasm, while FHC showed no detectable intracellular MMP-7. Interestingly, HEK293 cells showed a trace amount of MMP7 protein in the cytoplasm 581 compartment. Based on WB results, FHC normal colon epithelial cells and HCT-116 colon 582 cancer cells were treated with 125 μM pure EUG or 125 μM EUG delivered by casein-coated 583 NPs (Figure 10B). After 48 hours, cells were subjected to a crystal violet cell cytotoxicity assay 584 585 (Figure 10C and E). Supplementary Figure 1A-B shows validation of the cytotoxicity assay as 586 previously described [38]. The flow-chart in supplementary Figure 1C illustrates steps of the 587 crystal violet cell cytotoxicity assay. Figure 10 shows that 125 μM pure EUG had no effect on FHC cells while significantly decreasing the viability of HCT-116 cells (red columns versus blue 588 columns in panels D and F in Figure 10, respectively). Same concentration of EUG delivered by 589 casein-coated NPs further decreased cell viability in HCT-116 cancer cells (Figure 10F, green 590 591 column). Casein-coated NPs with and without EUG in FHC normal cells (Figure 10D, green and 592 purple columns) and casein-coated NPs without EUG in cancer cells (Figure 10F, purple column) increased the number of adherent cells due to the extra amount of available casein. As 593 594 previously reported, casein increases cellular adhesion through the E-cadherin/beta-catenin mechanism [73]. Based on the WB results (Figure 10A), we decided to examine the effect of 595

pure EUG and casein-coated NPs with EUG on HEK-293 cells. Supplementary Figure 1D-E shows that pure EUG had no effect on HEK-293 cells compared to DMSO (0.1% v/v) control group. Interestingly, EUG delivered with casein-coated NPs lead to significant reduction of cell viability in HEK-293 cells (green column). As it has been observed in HCT-116 and FHC cells (Figure 10), casein-coated NPs without EUG significantly increased cell adhesion in HEK-293 cells (Supplementary Figure 1E-purple column).

In the second set of experiments, HCT-116 and FHC cells were treated with casein-coated MSNs-FITC for 90 minutes, followed by confocal microscopy as previously described [41]. The results in Figure 10G and 10H indicate that HCT-116 colon cancer cells are associated with a substantial portion of NPs bound to the plasma membrane. We observed no association with, or internalization of NPs negatively charged MSN-FITC NPs with colon normal epithelial cells (Figure 10H). The Z-stack pictures in panels G -H (Figure 10) indicate a percentage of NPs-FITC internalized into the cytoplasm compartment of HCT-116 cells as previously described [75]. Results in Figure 10 suggest that the engineered casein-coated NPs in this study can selectively deliver and release an effective dose of their cargo (EUG) at tumor sites. At the same time, their low-affinity to normal cells with low or no active MMP-7 enzyme remain dominantly unexposed to high local concentrations of drugs.

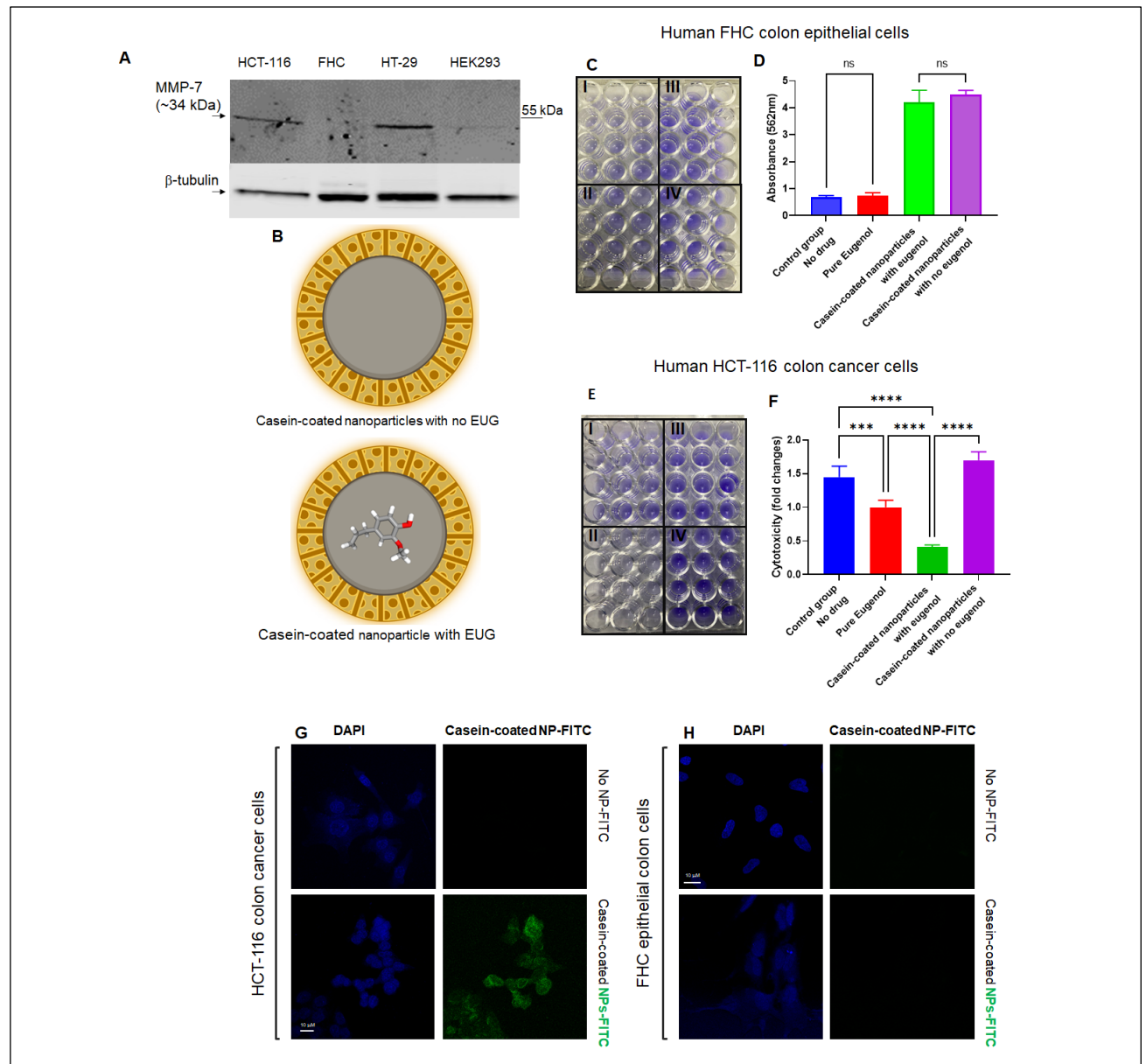


Figure 10: EUG delivered by casein-coated NP decreases cell viability in HCT-116 cells while FHC cells remain intact. (A) Anti-MMP-7 shows high expression of MMP-7 in colon cancer cells, while FHC cells showed no trace of intracellular MMP-7. HEK293 cells showed a trace of MMP-7. HCT-116 and FHC cells were treated with pure EUG (125μM), eosin-coated NPs without EUG, and casein-coated NPs with 125μM EUG (panel B) for 48 hours, followed by crystal cell viability assay. Panels C and E show the attached FHC and HCT-116 cells stained with crystal violet. I. Pure Eugenol, II. Casein-coated nanoparticles with EUG. III. Casein-coated nanoparticles with no eugenol and IV. control group (DMSO). Calculated results show that EUG significantly decreased cell viability in HCT-116 cells, while it has no effect on FHC cells (red column versus blue column in panels D and F. Delivery of 125mM EUG by NPs to HCT-116 cells further enhances the reduction of cell viability (green column in panel F). The casein-coated NPs without EUG increased the adherence of cells in HCT-116 and FHC (N=4 *****P<0.0001, mean ± SD). Panels G and H. HCT-116 and FHC were incubated with casein-coated MSNs-FITS (green signals) particles for 90 minutes and stained with DAPI (blue signals). The Z-stack images show only HCT-116 colon cancer cells have an affinity to MSNs,

and 90 minutes was enough for partial internalization of NPs to the cytoplasmic compartment. Scale bar is $10\mu M$).

Conclusions

CRC is the third leading cause of cancer death in the USA, with an estimated 52,000 deaths in 2022. Dissemination of primary tumor to distant sites such as the liver and lungs is the major cause of death in the majority of patients [76]. With limited therapeutic options for advanced CRC, there is a clear need to develop more effective targeted therapies to decrease the high mortality rates associated with metastatic disease [77]. According to current evidence, suppression of pathways involved in cell migration/invasion fed by epithelial-mesenchymal transition and inhibition of cancer stem cells can effectively slow down tumor metastasis in a broad range of cancer types, including CRC [78, 79]. However, despite the strong therapeutic potential of these tumorigenic targets, there are currently no effective targeted therapies. This study has explored the potential and underlying mechanisms role of a natural anti-cancer molecule, eugenol, for CRC therapeutics using a novel nanotechnology-based delivery system. Adequate drug concentrations of EUG delivered by casein-coated nanoparticles at the tumor site can effectively block severe undesirable side effects and decrease incidence of multiple drug resistance. Ultimately, this study provided a platform for a new generation of targeted therapies for patients with metastatic cancers.

 To further understand the anti-cancer mechanism of EUG against metastatic human colon cancer cells, cancer cells in different metastatic stages were treated with EUG. As the apoptotic effect of EUG in diverse malignant tumors was previously shown [45, 47, 80, 81], we demonstrated that EUG can induce early and late apoptosis in human colon cancer cells in a dose- and time dependent manner and significantly decreases cell migration and invasion, the two characteristic features used by metastatic cancer cells to invade adjacent tissues and metastasize to other organs [82]. We observed a similar inhibition in cell migration and invasion in the presence and the absence of FBS (starved versus non-starved conditions). Our results indicate that EUG interferes with major tumorigenic pathways involved in tumor metastasis such as KRAS pathway [83-85]. While the published data suggested that eugenol alone or its combination with cisplatin can target CSCs in breast and ovarian cancers, respectively [54, 55, 81], our set of flow-cytometry experiments revealed that a high dose of eugenol (500 μM) effectively decreases the population of CD44*, CD133* and LgR5* cells in a metastatic colon cancer cell line. It has been shown that

CD44 plays a key role in colon cancer invasion [86], while CD133 and Lgr5 cells are independent prognostic markers for low survival and drug-resistance in colon human colorectal cancer patients [87, 88]. The anti-CSCs effect of high dose of EUG further speaks to the therapeutic potential of casein-coated nanoparticles carrying high doses of EUG while minimizing its adverse effect on normal cells. Further studies will determine the underlying anti-cancer mechanism of EUG in CRC animal models using casein-coated NPs.

We engineered casein-coated mesoporous silica nanoparticles (EUG/CAS-MSNs-COOH) that efficiently encapsulate EUG, an anti-cancer drug molecule inside the MSN pore channels. We determined the optimal concentration of EUG to achieve efficient drug encapsulation efficiency and loading capacity by the MSN nanoassembly. We determined the optimum casein concentration that can efficiently trap the drug inside the particles. The release of EUG drug molecules from EUG/CAS-MSNs-COOH via enzymatic cleavage of the casein gatekeeping element (MMP-7 substrate) with trypsin proved the concept of the enzyme-triggered controlled release of EUG. Without a release-triggering enzyme, the EUG-loaded casein-capped MSNs did not exhibit any undesired EUG leakage at a wide range of pH values of the GI tract. It is well established that MMPs play an important role in the development and progression of CRC [67, 68], MMP-1, -2, -3, -7, -9, -13, and MT1-MMP are overexpressed in human CRC [69].. and their expression levels are associated with poor prognosis in CRC patients. Interestingly, EUG decreases the level of MMPs released by cancer cells [92] which indicate MMP-7triggered release of eugenol can be a self-regulated mechanism. This later effect can turn into a valuable bioactivatable probe specific for MMP activity by measuring MMP activity in CRC animal models treated with NPs-EUG versus typical chemotherapeutic drugs. Further, downregulation of MMP-7 expression by EUG may contribute to its suppressing effect on the migration and invasion of cancer cells, decreasing their aggressiveness.

We found that free EUG has no cytotoxic effect on either normal epithelial colon cells or on HEK-293 cells. In contrast, free EUG induced cytotoxicity in HCT-116 cells. Casein-coated and EUG-loaded NPs are more cytotoxic for colon cancer cells than free EUG, which reduces the drug's dose to achieve the same effect [93]. The traces of MMP-7 in HEK-293 cells and its tumorigenic characters [94] may account for the cytotoxicity of casein-coated and EUG-loaded NPs for those cells, which speaks to the expected role of MMP-7 in the release of EUG. The particles were not cytotoxic toward the normal FHC cell line. The enhanced effect of NPs delivering drug can be due to the different mode of cell penetration and consequent higher internalization resulting in high local concentrations of the drug at the tumor site. as previously described [95, 96]. Our confocal microscopy studies confirmed that casein-coated NPs labeled

with a fluorescent dye (FITC) had no affinity to FHC cells while they showed a high affinity and internalization in HCT-colon cancer cells.

Mechanistic studies of EUG delivered by an innovative use of nanotechnology for gated drug delivery will facilitate the development and clinical translation of NPs+EUG as new targeted therapies against primary and metastatic tumors.

700 701

696

697

698

699

702

- Supplementary Materials: The information on antibodies (Table S1) and validation of cytotoxicity assay (Supplementary Figure 1).
- 705 Acknowledgment and Funding
- The authors thank the National Institute of General Medical Sciences of the National Institutes
- of Health under Award Number U54GM128729 for financial support of this work, NSF-MRI
- 708 CHE-1337707 for the purchase of the SEM/EDX instrument, and the Department of Chemistry
- of the University of South Dakota. KR is supported by the National Cancer Institute of the
- National Institutes of Health under Award Number 1R03CA223935-01 as well as support by the
- 711 National Institute of General Medical Sciences of the National Institutes of Health under Award
- Number U54GM128729. Illustrator graphics were created with BioRender.com.

713

- Author Contributions: All authors contributed to designing, performing, or analyzing the
- experiments. The work was supervised by GS and KR and they wrote the manuscript. All authors
- 716 took part in editing the manuscript.

717

- 718 Institutional Review Board Statement: Not applicable.
- 719 Conflicts of Interest: The authors declare no conflict of interest.

720

721 722

References

- 723 1. Shao, R. G.; Cao, C. X.; Nieves-Neira, W.; Dimanche-Boitrel, M. T.; Solary, E.; Pommier, Y.,
- Activation of the Fas pathway independently of Fas ligand during apoptosis induced by camptothecin in p53 mutant human colon carcinoma cells. *Oncogene* **2001**, *20* (15), 1852-9.
- 726 2. Upreti, M.; Lyle, C. S.; Skaug, B.; Du, L.; Chambers, T. C., Vinblastine-induced apoptosis is
- mediated by discrete alterations in subcellular location, oligomeric structure, and activation status of
- 728 specific Bcl-2 family members. *J Biol Chem* **2006,** *281* (23), 15941-50.
- 3. Lichota, A.; Gwozdzinski, K., Anticancer Activity of Natural Compounds from Plant and Marine
- 730 Environment. Int J Mol Sci **2018**, 19 (11).

- 731 4. Islam, M. R.; Akash, S.; Rahman, M. M.; Nowrin, F. T.; Akter, T.; Shohag, S.; Rauf, A.; Aljohani, A.
- 732 S. M.; Simal-Gandara, J., Colon cancer and colorectal cancer: Prevention and treatment by potential
- 733 natural products. Chem Biol Interact 2022, 368, 110170.
- 734 5. Greenwell, M.; Rahman, P. K., Medicinal Plants: Their Use in Anticancer Treatment. *International*
- journal of pharmaceutical sciences and research **2015**, 6 (10), 4103-4112.
- 736 6. Li, M.; Zhao, G.; Su, W. K.; Shuai, Q., Enzyme-Responsive Nanoparticles for Anti-tumor Drug
- 737 Delivery. Frontiers in chemistry **2020**, *8*, 647.
- 738 7. Wang, X.; Teng, Z.; Wang, H.; Wang, C.; Liu, Y.; Tang, Y.; Wu, J.; Sun, J.; Wang, J.; Lu, G.,
- 739 Increasing the cytotoxicity of doxorubicin in breast cancer MCF-7 cells with multidrug resistance using a
- mesoporous silica nanoparticle drug delivery system. Int J Clin Exp Pathol 2014, 7 (4), 1337-47.
- 8. Bachiega, T. F.; de Sousa, J. P. B.; Bastos, J. K.; Sforcin, J. M., Clove and eugenol in noncytotoxic
- concentrations exert immunomodulatory/anti-inflammatory action on cytokine production by murine
- macrophages. *Journal of Pharmacy and Pharmacology* **2012,** *64* (4), 610-616.
- 744 9. Yoo, C.-B.; Han, K.-T.; Cho, K.-S.; Ha, J.; Park, H.-J.; Nam, J.-H.; Kil, U.-H.; Lee, K.-T., Eugenol
- isolated from the essential oil of Eugenia caryophyllata induces a reactive oxygen species-mediated
- apoptosis in HL-60 human promyelocytic leukemia cells. Cancer letters 2005, 225 (1), 41-52.
- 747 10. Benencia, F.; Courreges, M., In vitro and in vivo activity of eugenol on human herpesvirus.
- 748 Phytotherapy Research: An International Journal Devoted to Pharmacological and Toxicological
- 749 Evaluation of Natural Product Derivatives **2000**, 14 (7), 495-500.
- 750 11. Rossi, G. R.; Mautino, M. R.; Awwad, D. Z.; Husske, K.; Lejukole, H.; Koenigsfeld, M.; Ramsey, W.
- 751 J.; Vahanian, N.; Link, C. J., Allogeneic melanoma vaccine expressing αGal epitopes induces antitumor
- immunity to autologous antigens in mice without signs of toxicity. Journal of Immunotherapy 2008, 31
- 753 (6), 545-554.
- 754 12. Pramod, K.; Ansari, S. H.; Ali, J., Eugenol: a natural compound with versatile pharmacological
- actions. *Natural product communications* **2010,** *5* (12), 1934578X1000501236.
- 756 13. Series, W. H. O. J. W. T. R., Evaluation of certain food additives and contaminants. **2000**, (896).
- 757 14. Al-Sharif, I.; Remmal, A.; Aboussekhra, A., Eugenol triggers apoptosis in breast cancer cells
- 758 through E2F1/survivin down-regulation. *BMC cancer* **2013**, *13* (1), 1-10.
- 759 15. Fischer, I. U.; von Unruh, G. E.; Dengler, H. J., The metabolism of eugenol in man. *Xenobiotica*;
- the fate of foreign compounds in biological systems **1990**, 20 (2), 209-22.
- 761 16. Slamenová, D.; Horváthová, E.; Wsólová, L.; Sramková, M.; Navarová, J., Investigation of anti-
- oxidative, cytotoxic, DNA-damaging and DNA-protective effects of plant volatiles eugenol and borneol in
- 763 human-derived HepG2, Caco-2 and VH10 cell lines. Mutat Res 2009, 677 (1-2), 46-52.
- 764 17. Wright, S. E.; Baron, D. A.; Heffner, J. E., Intravenous eugenol causes hemorrhagic lung edema in
- 765 rats: proposed oxidant mechanisms. The Journal of laboratory and clinical medicine 1995, 125 (2), 257-
- 766 64.
- 767 18. Soundran, V.; Namagiri, T.; Manonayaki, S.; Vanithakumari, G., Hepatotoxicity of eugenol.
- 768 Ancient science of life **1994**, 13 (3-4), 213-7.
- 769 19. Vallet-Regi, M.; Ramila, A.; Del Real, R.; Pérez-Pariente, A new property of MCM-41: drug
- 770 delivery system. *Chem. Mater.* **2001,** *13* (2), 308-311.
- 771 20. Tang, F.; Li, L.; Chen, D., Mesoporous silica nanoparticles: synthesis, biocompatibility and drug
- 772 delivery. J. Adv. Mater. **2012**, 24 (12), 1504-1534.
- 773 21. Florek, J.; Caillard, R.; Kleitz, F., Evaluation of mesoporous silica nanoparticles for oral drug
- delivery–current status and perspective of MSNs drug carriers. *Nanoscale* **2017**, *9* (40), 15252-15277.
- 775 22. Wu, S.-H.; Hung, Y.; Mou, C.-Y. J. C. C., Mesoporous silica nanoparticles as nanocarriers.
- 776 *ChemComm* **2011,** *47* (36), 9972-9985.
- 777 23. Vallet-Regi, M.; Colilla, M.; Izquierdo-Barba, I.; Manzano, M., Mesoporous Silica Nanoparticles
- for Drug Delivery: Current Insights. *Molecules* **2017**, *23* (1).

- 779 24. Fernandez-Fernandez, A.; Manchanda, R.; McGoron, A. J., Theranostic applications of
- 780 nanomaterials in cancer: drug delivery, image-guided therapy, and multifunctional platforms. Appl.
- 781 *Biochem. Biotechnol.* **2011,** *165* (7-8), 1628-1651.
- 782 25. M Rosenholm, J.; Sahlgren, C.; Lindén, M., Multifunctional mesoporous silica nanoparticles for
- 783 combined therapeutic, diagnostic and targeted action in cancer treatment. *Curr. Drug Targets* **2011,** *12*
- 784 (8), 1166-1186.
- 785 26. Baeza, A.; Colilla, M.; Vallet-Regí, M., Advances in mesoporous silica nanoparticles for targeted
- stimuli-responsive drug delivery. Expert Opin. Drug Delivery 2015, 12 (2), 319-337.
- 787 27. Argyo, C.; Weiss, V.; Bräuchle, C.; Bein, T., Multifunctional mesoporous silica nanoparticles as a
- vniversal platform for drug delivery. Chemistry of Materials 2014, 26 (1), 435-451.
- 789 28. Martínez-Carmona, M.; Colilla, M.; Vallet-Regí, M., Smart mesoporous nanomaterials for
- 790 antitumor therapy. *J. Nanomater.* **2015,** *5* (4), 1906-1937.
- 791 29. Castillo, R. R.; Colilla, M.; Vallet-Regí, M., Advances in mesoporous silica-based nanocarriers for
- 792 co-delivery and combination therapy against cancer. Expert Opin. Drug Delivery 2017, 14 (2), 229-243.
- 793 30. Zhao, Y.; Trewyn, B. G.; Slowing, II; Lin, V. S., Mesoporous silica nanoparticle-based double drug
- delivery system for glucose-responsive controlled release of insulin and cyclic AMP. J Am Chem Soc
- 795 **2009,** *131* (24), 8398-400.
- 796 31. Popat, A.; Ross, B. P.; Liu, J.; Jambhrunkar, S.; Kleitz, F.; Qiao, S. Z., Enzyme-responsive controlled
- 797 release of covalently bound prodrug from functional mesoporous silica nanospheres. Angew. Chem., Int.
- 798 *Ed.* **2012,** *51* (50), 12486-9.
- 799 32. Kumar, B.; Kulanthaivel, S.; Mondal, A.; Mishra, S.; Banerjee, B.; Bhaumik, A.; Banerjee, I.; Giri,
- 800 S.; Biointerfaces, S. B., Mesoporous silica nanoparticle based enzyme responsive system for colon
- specific drug delivery through guar gum capping. *Colloids Surf.* **2017,** *150*, 352-361.
- 802 33. Garg, P.; Sarma, D.; Jeppsson, S.; Patel, N. R.; Gewirtz, A. T.; Merlin, D.; Sitaraman, S. V., Matrix
- metalloproteinase-9 functions as a tumor suppressor in colitis-associated cancer. *Cancer Res* **2010,** *70*
- 804 (2), 792-801.
- 805 34. Packard, B. Z.; Artym, V. V.; Komoriya, A.; Yamada, K. M., Direct visualization of protease activity
- on cells migrating in three-dimensions. *Matrix biology : journal of the International Society for Matrix*
- 807 Biology 2009, 28 (1), 3-10.
- 808 35. Zeng, Z.-S.; Shu, W.-P.; Cohen, A. M.; Guillem, J. G., Matrix Metalloproteinase-7 Expression in
- 809 Colorectal Cancer Liver Metastases. Clinical Cancer Research 2002, 8 (1), 144.
- 810 36. Wang, J.; Wang, Y.; Liu, Q.; Yang, L.; Zhu, R.; Yu, C.; Wang, S., Rational Design of Multifunctional
- 811 Dendritic Mesoporous Silica Nanoparticles to Load Curcumin and Enhance Efficacy for Breast Cancer
- 812 Therapy. *ACS applied materials & interfaces* **2016**, *8* (40), 26511-26523.
- 813 37. Sane, S.; Hafner, A.; Srinivasan, R.; Masood, D.; Slunecka, J. L.; Noldner, C. J.; Hanson, A. D.;
- Kruisselbrink, T.; Wang, X.; Wang, Y.; Yin, J.; Rezvani, K., UBXN2A enhances CHIP-mediated proteasomal
- degradation of oncoprotein mortalin-2 in cancer cells. Molecular oncology 2018.
- 816 38. Sane, S.; Abdullah, A.; Boudreau, D. A.; Autenried, R. K.; Gupta, B. K.; Wang, X.; Wang, H.;
- Schlenker, E. H.; Zhang, D.; Telleria, C.; Huang, L.; Chauhan, S. C.; Rezvani, K., Ubiquitin-like (UBX)-
- domain-containing protein, UBXN2A, promotes cell death by interfering with the p53-Mortalin
- interactions in colon cancer cells. *Cell Death Dis* **2014**, *5*, e1118.
- 820 39. Edwards, G.; Campbell, T.; Henderson, V.; Danaher, A.; Wu, D.; Srinivasan, R.; Rezvani, K.; Odero-
- Marah, V. A., SNAIL Transctiption factor in prostate cancer cells promotes neurite outgrowth. *Biochimie*
- 822 **2021,** *180,* 1-9.
- 823 40. Kho, D.; MacDonald, C.; Johnson, R.; Unsworth, C. P.; #039; Carroll, S. J.; Mez, E. D.; Angel, C. E.;
- 824 Graham, E. S., Application of xCELLigence RTCA Biosensor Technology for Revealing the Profile and
- Window of Drug Responsiveness in Real Time. **2015**, *5* (2), 199-222.

- 826 41. Wijewantha, N.; Eikanger, M. M.; Antony, R. M.; Potts, R. A.; Rezvani, K.; Sereda, G., Targeting
- 827 Colon Cancer Cells with Enzyme-Triggered Casein-Gated Release of Cargo from Mesoporous Silica-Based
- 828 Nanoparticles. *Bioconjugate Chemistry* **2021,** *32* (11), 2353-2365.
- 829 42. Carneiro, B. A.; El-Deiry, W. S., Targeting apoptosis in cancer therapy. Nat Rev Clin Oncol 2020,
- 830 *17* (7), 395-417.
- 831 43. Wang, Y.; Zhong, J.; Bai, J.; Tong, R.; An, F.; Jiao, P.; He, L.; Zeng, D.; Long, E.; Yan, J.; Yu, J.; Cai, L.,
- The Application of Natural Products in Cancer Therapy by Targeting Apoptosis Pathways. *Current drug*
- 833 *metabolism* **2018,** *19* (9), 739-749.
- 834 44. Kittakoop, P.; Mahidol, C.; Ruchirawat, S., Alkaloids as important scaffolds in therapeutic drugs
- for the treatments of cancer, tuberculosis, and smoking cessation. Curr Top Med Chem 2014, 14 (2), 239-
- 836 52.
- 45. Jaganathan, S. K.; Mazumdar, A.; Mondhe, D.; Mandal, M., Apoptotic effect of eugenol in human
- colon cancer cell lines. *Cell Biol Int* **2011,** *35* (6), 607-15.
- 46. Fathy, M.; Fawzy, M. A.; Hintzsche, H.; Nikaido, T.; Dandekar, T.; Othman, E. M., Eugenol Exerts
- Apoptotic Effect and Modulates the Sensitivity of HeLa Cells to Cisplatin and Radiation. *Molecules (Basel,*
- 841 Switzerland) **2019,** 24 (21).
- 842 47. Al-Sharif, I.; Remmal, A.; Aboussekhra, A., Eugenol triggers apoptosis in breast cancer cells
- through E2F1/survivin down-regulation. *BMC Cancer* **2013**, *13*, 600.
- 48. Yeung, T. M.; Gandhi, S. C.; Wilding, J. L.; Muschel, R.; Bodmer, W. F., Cancer stem cells from
- colorectal cancer-derived cell lines. Proc Natl Acad Sci U S A 2010, 107 (8), 3722-7.
- 846 49. Maamer-Azzabi, A.; Ndozangue-Touriguine, O.; Bréard, J., Metastatic SW620 colon cancer cells
- are primed for death when detached and can be sensitized to anoikis by the BH3-mimetic ABT-737. Cell
- 848 Death Dis **2013**, 4 (9), e801.
- 849 50. van Zijl, F.; Krupitza, G.; Mikulits, W., Initial steps of metastasis: cell invasion and endothelial
- 850 transmigration. *Mutat Res* **2011,** *728* (1-2), 23-34.
- 851 51. Hamidi, H.; Lilja, J.; Ivaska, J., Using xCELLigence RTCA Instrument to Measure Cell Adhesion. Bio
- 852 *Protoc* **2017,** *7* (24), e2646.
- 52. Limame, R.; Wouters, A.; Pauwels, B.; Fransen, E.; Peeters, M.; Lardon, F.; De Wever, O.;
- Pauwels, P., Comparative analysis of dynamic cell viability, migration and invasion assessments by novel
- real-time technology and classic endpoint assays. *PLoS One* **2012**, *7* (10), e46536.
- 856 53. Wang, C.; Xie, J.; Guo, J.; Manning, H. C.; Gore, J. C.; Guo, N., Evaluation of CD44 and CD133 as
- cancer stem cell markers for colorectal cancer. Oncol Rep 2012, 28 (4), 1301-8.
- 858 54. Choudhury, P.; Barua, A.; Roy, A.; Pattanayak, R.; Bhattacharyya, M.; Saha, P., Eugenol restricts
- 859 Cancer Stem Cell population by degradation of β-catenin via N-terminal Ser37 phosphorylation-an in
- vivo and in vitro experimental evaluation. *Chem Biol Interact* **2020**, *316*, 108938.
- 861 55. Islam, S. S.; Al-Sharif, I.; Sultan, A.; Al-Mazrou, A.; Remmal, A.; Aboussekhra, A., Eugenol
- 862 potentiates cisplatin anti-cancer activity through inhibition of ALDH-positive breast cancer stem cells
- and the NF-κB signaling pathway. *Mol Carcinog* **2018**, *57* (3), 333-346.
- 864 56. Wang, X. F.; Zhang, X. L.; Xu, L. P.; Shi, G. G.; Zheng, H. Y.; Sun, B. C., [Expression of stem cell
- markers CD44 and Lgr5 in colorectal cancer and its relationship with lymph node and liver metastasis].
- 866 Zhonghua yi xue za zhi **2018,** 98 (36), 2899-2904.
- 867 57. Ren, F.; Sheng, W.-Q.; Du, X., CD133: a cancer stem cells marker, is used in colorectal cancers.
- 868 *World journal of gastroenterology* **2013,** *19* (17), 2603-2611.
- 869 58. Ma, Y.-S.; Li, W.; Liu, Y.; Shi, Y.; Lin, Q.-L.; Fu, D., Targeting Colorectal Cancer Stem Cells as an
- 870 Effective Treatment for Colorectal Cancer. *Technology in Cancer Research & Treatment* **2020,** 19,
- 871 1533033819892261.
- 872 59. Wijewantha, N. L. W. Design of Biocompatible Mineral Materials for Drug Delivery. University of
- 873 South Dakota, 2020.

- 874 60. Luo, Z.; Cai, K.; Hu, Y.; Zhao, L.; Liu, P.; Duan, L.; Yang, W., Mesoporous silica nanoparticles end-
- 875 capped with collagen: redox-responsive nanoreservoirs for targeted drug delivery. *Angew Chem Int Ed*
- 876 Engl **2011**, 50 (3), 640-3.
- 877 61. Woranuch, S.; Yoksan, R., Eugenol-loaded chitosan nanoparticles: I. Thermal stability
- improvement of eugenol through encapsulation. *Carbohydrate polymers* **2013**, *96* (2), 578-585.
- 62. Chen, H.; Chen, L.; Shen, Z.; Zhou, H.; Hao, L.; Xu, H.; Zhou, X., Synthesis of mesoporous silica
- post-loaded by methyl eugenol as an environment-friendly slow-release bio pesticide. *Scientific reports*
- 881 **2020,** *10* (1), 1-12.
- 882 63. Chakrapani, V.; Ahmed, K. B. A.; Kumar, V. V.; Ganapathy, V.; Anthony, S. P.; Anbazhagan, V., A
- facile route to synthesize casein capped copper nanoparticles: an effective antibacterial agent and
- selective colorimetric sensor for mercury and tryptophan. RSC Advances 2014, 4 (63), 33215-33221.
- 885 64. Fallingborg, J., Intraluminal pH of the human gastrointestinal tract. *Danish medical bulletin* **1999**,
- 886 *46* (3), 183-196.
- 887 65. Nugent, S.; Kumar, D.; Rampton, D.; Evans, D., Intestinal luminal pH in inflammatory bowel
- disease: possible determinants and implications for therapy with aminosalicylates and other drugs. *Gut*
- 889 **2001,** *48* (4), 571-577.
- 890 66. Beasley, D. E.; Koltz, A. M.; Lambert, J. E.; Fierer, N.; Dunn, R. R., The evolution of stomach
- acidity and its relevance to the human microbiome. *PloS one* **2015**, *10* (7), e0134116.
- 892 67. Mysliwiec, A. G.; Ornstein, D. L., Matrix Metalloproteinases in Colorectal Cancer. *Clinical*
- 893 *colorectal cancer* **2002,** *1* (4), 208-219.
- 894 68. Jeong Eun, S.; M.D.[†]; Sung-Ae, J.; M.D; Seong-Eun, K.; M.D; Yang-Hee, J.; Ki-Nam, S.; M.D; Tae
- Hun, K.; M.D; Kwon, Y.; M.D; Il-Hwan, M.; M.D, Expression of Matrix Metalloproteinase in Colon
- 896 Adenoma and Colon Cancer: MT1-MMP and TIMP-2. *Intest Res* **2007**, *5* (2), 144-150.
- 897 69. Zucker, S.; Vacirca, J., Role of matrix metalloproteinases (MMPs) in colorectal cancer. *Cancer*
- 898 Metastasis Rev 2004, 23 (1-2), 101-17.
- 899 70. Kumar, A.; Collins, H.; Van Tam, J.; Scholefield, J. H.; Watson, S. A., Effect of preoperative
- radiotherapy on matrilysin gene expression in rectal cancer. *European Journal of Cancer* **2002,** *38* (4),
- 901 505-510.
- 902 71. POLISTENA, A.; CUCINA, A.; DINICOLA, S.; STENE, C.; CAVALLARO, G.; CIARDI, A.; ORLANDO, G.;
- 903 ARENA, R.; D'ERMO, G.; CAVALLARO, A.; JOHNSON, L. B.; DE TOMA, G., MMP7 Expression in Colorectal
- 904 Tumours of Different Stages. In Vivo 2014, 28 (1), 105-110.
- 905 72. Scherer, R. L.; VanSaun, M. N.; McIntyre, J. O.; Matrisian, L. M., Optical imaging of matrix
- metalloproteinase-7 activity in vivo using a proteolytic nanobeacon. *Molecular imaging* **2008,** *7* (3), 118-
- 907 131.
- 908 73. Lickert, H.; Bauer, A.; Kemler, R.; Stappert, J., Casein kinase II phosphorylation of E-cadherin
- increases E-cadherin/beta-catenin interaction and strengthens cell-cell adhesion. J Biol Chem 2000, 275
- 910 (7), 5090-5.
- 911 74. Wijewantha, N.; Eikanger, M. M.; Antony, R. M.; Potts, R. A.; Rezvani, K.; Sereda, G., Targeting
- 912 Colon Cancer Cells with Enzyme-Triggered Casein-Gated Release of Cargo from Mesoporous Silica-Based
- 913 Nanoparticles. *Bioconjugate chemistry* **2021,** *32* (11), 2353-2365.
- 914 75. Manzanares, D.; Ceña, V., Endocytosis: The Nanoparticle and Submicron Nanocompounds
- 915 Gateway into the Cell. *Pharmaceutics* **2020,** *12* (4).
- 916 76. Hu, Z.; Ding, J.; Ma, Z.; Sun, R.; Seoane, J. A.; Scott Shaffer, J.; Suarez, C. J.; Berghoff, A. S.;
- 917 Cremolini, C.; Falcone, A.; Loupakis, F.; Birner, P.; Preusser, M.; Lenz, H. J.; Curtis, C., Quantitative
- 918 evidence for early metastatic seeding in colorectal cancer. Nat Genet 2019, 51 (7), 1113-1122.
- 919 77. Xie, Y.-H.; Chen, Y.-X.; Fang, J.-Y., Comprehensive review of targeted therapy for colorectal
- 920 cancer. Signal Transduction and Targeted Therapy **2020,** 5 (1), 22.

- 921 78. Ma, Y. S.; Li, W.; Liu, Y.; Shi, Y.; Lin, Q. L.; Fu, D., Targeting Colorectal Cancer Stem Cells as an
- 922 Effective Treatment for Colorectal Cancer. Technol Cancer Res Treat 2020, 19, 1533033819892261.
- 923 79. Zhang, N.; Ng, A. S.; Cai, S.; Li, Q.; Yang, L.; Kerr, D., Novel therapeutic strategies: targeting
- 924 epithelial-mesenchymal transition in colorectal cancer. Lancet Oncol 2021, 22 (8), e358-e368.
- 925 80. Majeed, H.; Antoniou, J.; Fang, Z., Apoptotic effects of eugenol-loaded nanoemulsions in human
- olon and liver cancer cell lines. Asian Pac J Cancer Prev 2014, 15 (21), 9159-64.
- 927 81. Islam, S. S.; Aboussekhra, A., Sequential combination of cisplatin with eugenol targets ovarian
- oancer stem cells through the Notch-Hes1 signalling pathway. J Exp Clin Cancer Res 2019, 38 (1), 382.
- 929 82. Wu, J.-s.; Jiang, J.; Chen, B.-j.; Wang, K.; Tang, Y.-l.; Liang, X.-h., Plasticity of cancer cell invasion:
- 930 Patterns and mechanisms. *Translational Oncology* **2021,** *14* (1), 100899.
- 931 83. Porru, M.; Pompili, L.; Caruso, C.; Biroccio, A.; Leonetti, C., Targeting KRAS in metastatic
- olorectal cancer: current strategies and emerging opportunities. J Exp Clin Cancer Res 2018, 37 (1), 57.
- 933 84. Li, Z.; Veeraraghavan, V. P.; Mohan, S. K.; Bolla, S. R.; Lakshmanan, H.; Kumaran, S.; Aruni, W.;
- Aladresi, A. A. M.; Shair, O. H. M.; Alharbi, S. A.; Chinnathambi, A., Apoptotic induction and anti-
- 935 metastatic activity of eugenol encapsulated chitosan nanopolymer on rat glioma C6 cells via alleviating
- the MMP signaling pathway. *J Photochem Photobiol B* **2020,** 203, 111773.
- 937 85. Sarkar, A.; Das, S.; Rahaman, A.; Das Talukdar, A.; Bhattacharjee, S.; Mandal, D. P., Eugenol and
- 938 capsaicin exhibit anti-metastatic activity via modulating TGF-β signaling in gastric carcinoma. Food &
- 939 function **2020**, 11 (10), 9020-9034.
- 940 86. Cho, S. H.; Park, Y. S.; Kim, H. J.; Kim, C. H.; Lim, S. W.; Huh, J. W., CD44 enhances the epithelial-
- mesenchymal transition in association with colon cancer invasion. *Int J Oncol* **2012,** *41*.
- 942 87. Horst, D.; Kriegl, L.; Engel, J.; Kirchner, T.; Jung, A., CD133 expression is an independent
- prognostic marker for low survival in colorectal cancer. *British Journal of Cancer* **2008**, *99* (8), 1285-1289.
- 944 88. Hsu, H. C.; Liu, Y. S.; Tseng, K. C.; Hsu, C. L.; Liang, Y.; Yang, T. S.; Chen, J. S.; Tang, R. P.; Chen, S.
- J.; Chen, H. C., Overexpression of Lgr5 correlates with resistance to 5-FU-based chemotherapy in
- 946 colorectal cancer. *Int J Colorectal Dis* **2013**, *28* (11), 1535-46.
- 947 89. Soleyman-Jahi, S.; Nedjat, S.; Abdirad, A.; Hoorshad, N.; Heidari, R.; Zendehdel, K., Prognostic
- 948 significance of matrix metalloproteinase-7 in gastric cancer survival: a meta-analysis. *PloS one* **2015**, *10*
- 949 (4), e0122316-e0122316.
- 950 90. Polistena, A.; Cucina, A.; Dinicola, S.; Stene, C.; Cavallaro, G.; Ciardi, A.; Orlando, G.; Arena, R.;
- 951 D'Ermo, G.; Cavallaro, A.; Johnson, L. B.; De Toma, G., MMP7 expression in colorectal tumours of
- 952 different stages. *In Vivo* **2014,** *28* (1), 105-10.
- 953 91. Visse, R.; Nagase, H., Matrix metalloproteinases and tissue inhibitors of metalloproteinases:
- structure, function, and biochemistry. *Circ Res* **2003**, *92* (8), 827-39.
- 95. Shweta Rajoriya, N. P., Karthik KV, Ajay Kumar, Mohini Saini and Meena Kataria. , Study on
- effect of eugenol on anti-metastatic activity and expression of MMPS in TNBC MDA MB: 231 cell line. J
- 957 *Pharmacogn Phytochem* **2019**, *8* (4), 788-794.
- 958 93. Benyettou, F.; Fahs, H.; Elkharrag, R.; Bilbeisi, R. A.; Asma, B.; Rezgui, R.; Motte, L.; Magzoub, M.;
- 959 Brandel, J.; Olsen, J. C.; Piano, F.; Gunsalus, K. C.; Platas-Iglesias, C.; Trabolsi, A., Selective growth
- 960 inhibition of cancer cells with doxorubicin-loaded CB[7]-modified iron-oxide nanoparticles. RSC
- 961 Advances **2017**, 7 (38), 23827-23834.
- 962 94. Stepanenko, A. A.; Dmitrenko, V. V., HEK293 in cell biology and cancer research: phenotype,
- karyotype, tumorigenicity, and stress-induced genome-phenotype evolution. Gene 2015, 569 (2), 182-
- 964 90.
- 965 95. Huwyler, J.; Cerletti, A.; Fricker, G.; Eberle, A. N.; Drewe, J., By-passing of P-glycoprotein using
- 966 immunoliposomes. *J Drug Target* **2002,** *10* (1), 73-9.
- 96. Gabizon, A.; Shmeeda, H.; Barenholz, Y., Pharmacokinetics of pegylated liposomal Doxorubicin:
- 968 review of animal and human studies. *Clinical pharmacokinetics* **2003**, *42* (5), 419-36.